LIST OF CONTENTS

List of tables

Table

List of figures

List of Abbreviations

EHP	Electron hole pair
EQE	External quantum efficiency
FF.	Fill factor
I_{SC}	Short circuit current
IQE	Internal quantum efficiency
J_{SC}	Short circuit current density
MoS_2	Molybdenum disulphide
N_C/N_V	Conduction and valence band density of states
N_D/N_A	Donor and acceptor concentration
PCE	Power conversion efficiency
TCE	Transparent conducting electrode
TCO	Transparent conducting oxide
TMCD	Transition metal dichalcogenides
WSe_2	Tungsten diselenide
SWR	Spectral response
V_{OC}	Open circuit voltage
2D	Two dimensional

Chapter 1 : Introduction

1.1 Thesis statement

In this work, we are proposing a silicon heterojunction solar cell model and the simulations have been carried out using AFORS-HET software. The model uses multilayer tungsten diselenide (WSe_2), a member of transition dichalcogenides (TMCDs), as the top layer of the solar cell, which is also serving as a transparent conducting electrode (TCE). Various parameters of different layers have been optimized to obtain maximum efficiency. The results have been analyzed graphically and finally obtained values of solar cell output parameters, along with the respective optimized values have been tabulated.

1.2 Thesis objective

This project has been carried out with to fulfill the following objectives –

- Simulation of WSe_2/silicon heterojunction solar cell and study of its V-I characteristics.
- Study of various material parameters and their effect on solar cell output results.
- Study of varying number of layers of WSe_2 from trilayer to 40 layers on the top layer and its consequent effect on power conversion efficiency (PCE).
- Study of variation in output parameters with the change in temperature.
- Analysis of spectral response , internal quantum efficiency(IQE) and external quantum efficiency(EQE) of the WSe_2-pcSi optimized solar cell.

1.3 Thesis organization

The final results of the simulations carried out in this project have been organized in 9 chapters. Chapter 1 is the introduction part consisting of statement and goal of this thesis. It gives general information of all the objectives briefly which are covered in this work. Chapter 2 deals with the basics of solar cells and solar spectrum. Solar cell output characteristics can be described by short circuit current (Isc), open circuit voltage (VOC) , fill factor (FF) and power conversion efficiency (PCE) . These parameters are explained in detail along with the factors affecting them.

Chapter 3, is about the three generations of silicon based solar cells. Each of them has some advantages and disadvantages regarding the cost and efficiency of device.

The third generation of solar cell is heterojunction solar cells which uses best of both first and second generation solar cells. As, this thesis deals with simulation of heterojunction solar cells, they have been discussed in detail along with their working , types of hetero structures , formation of band diagram and quasi Fermi levels in hetero structure.

Chapter 4 gives the basic solar cell features. For being used as a solar cell component, the material should posses some special electrical, optical, environment friendly features for maximum PCE and minimum cost of production and maintenance. These properties of ideal solar cell material are discussed briefly in this chapter. Further the interface between two different semiconductors could be either ohmic or schottky which is discussed in chapter 4.6

And finally, the three basic recombination models are explained which limits the solar cell efficiencies to very large extent.

Chapter 5 is the literature review to all previous works done in heterojunction solar cells and the motivation behind this project. It also gives a brief introduction to transition metal dichalcogenides (TMCDs) along with their physical, chemical and electrical properties. Chapter 6 is the brief introduction to AFORS-HET software and involves the basic steps of simulation carried out. Further, it defines the proposed solar structure for simulation along with its band diagram.

Chapter 7 is the detailed analysis of results obtained from simulation. All the layer parameters for both the semiconductors have been varied in fixed reported ranges and their effect on Isc, Voc, FF and PCE have been studied here. We have also analyzed the effect of layer number of WSe_2 on the output of solar cell. Moreover, we have studied the effect of temperature on solar cell along with its spectral response, internal quantum efficiency and external quantum efficiency. Chapter 8 is the conclusion part along with the best optimized solar cell parameters under various simulation conditions.

Chapter 9 is the reference section citing all the references used in the thesis writing.

Chapter 2 : Solar energy and solar cells

2.1 Solar cells

Solar cell is an electrical device that converts solar energy directly to electrical energy using the photovoltaic phenomenon and produces an output when exposed to sunlight by varying its electrical characteristics. Today, in the present world of growing demands, solar cells are the most energy efficient and economical devices in which sunlight is used as an input to produce an output that could run power equipments, electrical devices as well as recharge batteries. They are made up of semiconductor materials such as silicon, GaAs etc. They demand very low maintenance and serve as a non- polluting, silent and sustainable source of electrical energy. Historically, solar cells were used in remote area power systems where electrical power from grid was unavailable but now a days, solar cells are being used in almost all areas whether commercial or non commercial. Some of the numerous areas where solar cells are being implemented in day-today life are satellite power system, water treatment system, remote lighting system, rechargeable batteries, watches, electrical fences and calculators.

The power conversion efficiency of solar cells depends on the type and the area of materials used for different layers, wavelength and intensity of sunlight. Fundamentally, the solar to electrical conversion takes place in two basic steps i.e, absorption and conversion of photons to electron hole pair(EHP) and secondly the separation of charge carriers using built-in potential to some conductive contacts that transmits them to generate electricity.

2.2 Standardized Solar Spectrum and Air mass

Solar energy is a result of numerous nuclear fusion reactions taking place in the core of sun. The core of sun has huge amount of hydrogen atoms that account for 74.9% of sun's mass, which stick together to form helium atoms by nuclear fusion reaction. This exothermic chemical reaction gives out immense energy which moves across the solar system .This released energy from the core of sun has to travel several layers of solar photosphere before escaping as sunlight in the solar system.

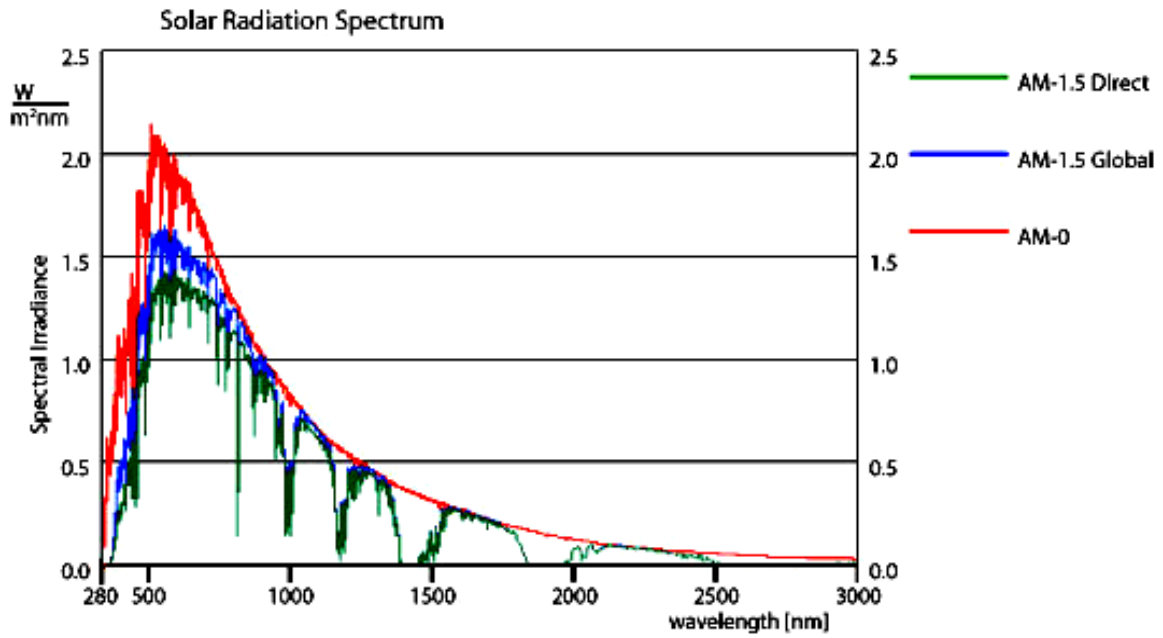

Figure 2.1 Solar radiation spectrum [1]

The solar electromagnetic radiations striking earth ,consists of a wide band of wavelengths ranging from 250 nm to 1 mm which is mainly ultraviolet waves(A,B,C) , infrared waves and visible light. After striking the earth's outer layer, some of the UV rays gets filtered while the other portion passes through it.

The PCE of a photovoltaic device largely depends on the wavelength and intensity of sunlight striking it. For obtaining an accurate and precise comparison of various solar cells measured at different times of day and at differing locations, some standards have been defined for solar spectrum and power density being radiated to earth's atmosphere as well as outside the earth's atmosphere.

For the purpose of defining standard solar spectrum, air mass (AM) coefficient is used as shown in figure 2.1. Air mass can be defined as portion of atmosphere that the sunlight must pass through before striking the earth's surface relative to its overhead path length. Using the air mass coefficient, the following standard spectrums are defined:

AM0 – The spectrum for outside the earth is defined as AM0, because in this case the sunlight does not pass through any stage of earth's atmosphere. It signifies the power density of 1366.1W/m^2 . AM0 is used for space power applications such as satellite's power system.

AM 1 – The spectrum travelling 1 atmosphere overhead directly to the sea level is known as standard spectrum AM1 which is useful in analyzing solar cell performance in equatorial and tropical regions of earth.

AM1.5- For the inner Earth's surface, the standard solar spectrum is defined as AM1.5G of AM1.5D ,where G stands for global and includes direct as well as diffuse radiations whereas D stands for direct radiation only. The power density for AM1.5D can be approximated by cutting the AM0 by 28% out of which 18% accounts for absorption while the other 10% accounts for scattering. Hence, the intensity comes out to be 970 W/m^2 which is rounded off to 1000 W/m^2 for convenience purpose.

AM2:3 –This solar spectrum is used to analyze performance of solar cells at higher and temperate latitudes.

AM 38 – This solar spectrum accounts for horizontal sea level i.e, 90 degrees from the overhead position, however it is known to have some variations.

2.3 Electrical characteristics of a solar cell –

Solar cell is very large p-n junction diode, hence an ideal solar cell can be represented by electrical circuit having a ideal current source in parallel to a diode along with a series resistance R_S and shunt resistance R_{SH} as shown in Figure 2.2 below.

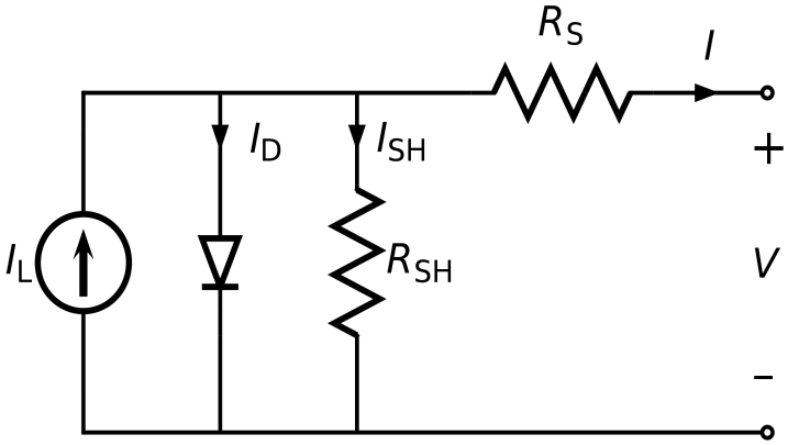

Figure 2.2 Electrical equivalent of solar cell

The total output current can hence be given as below,

$$I=I_L-I_D \quad (1)$$

where I_L is the photo generated current; I_D is the diode current and I_{SH} being the shunt leakage current. The diode current I_D is given as,

$$I_D = Io\left[\exp\left(\frac{qV}{kT}\right) - 1\right] \quad (2)$$

Where Io is the saturation current of diode, q is the charge,V is the diode forward bias voltage ,k is boltzman constant and T being the temperature in kelvin. If solar cell is considered ideal, then I_{SH} =0, and the output current can be written as

$$I=I_L- Io\left[\exp\left(\frac{qV}{kT}\right) - 1\right] \quad (3)$$

Short circuit current Isc -

Short circuit current is the maximum current flowing through the circuit when the load is not connected i.e, when no bias voltage has been applied. When a load is connected, there occurs some voltage drop and hence maximal current can't be obtained. Short circuit current is only contributed by the light generated carriers (electrons). For an ideal solar cell with minimal recombination and losses, the short circuit current and the light generated currents are almost similar. Isc depends on various factors which are discussed below-

Total area of solar cell-The short circuit current is almost directly proportional to the solar cell's area . Hence, in order to compare the various solar cells with varying areas, the short circuit current is normalized and instead short circuit current density is used as a characteristic parameter.

$$Jsc = \frac{Isc}{Area} \quad (4)$$

$$J=J_{sc}-Jo\left[\exp\left(\frac{qV}{kT}\right) - 1\right] \quad (5)$$

Effect of incident light-The short circuit current, Isc also depends on the intensity of incident light ,i.e. number of photons striking the solar cell. Higher the number of photons striking, larger

would be the EHP generation which would increase the light generated current and eventually the short circuit current.

Wavelength of incident light-The number of free electron-hole pairs generated also depend largely on the wavelength and the power density of light. This has been standardized in using various air mass coefficients. The standard spectrum used mostly is AM1.5 with the rounded off power density of $1000W/m^2$.

Optoelectronic properties of absorber material- The photo absorption and the photo conversion process largely depend upon the absorber material's properties. Various layers above the absorber and the absorber layer should have high absorption coefficient with minimal losses. Mostly, a direct band gap material is preferred as it has an ease for photon to electron conversion.

Minority carrier lifetime-The process of mere generation of charge carriers does not account for current, rather the current flows when these generated carriers are collected at the conductive terminals of circuit. For the carriers to reach the terminals, they should have appreciable lifetime which can be obtained by various techniques that reduce carrier recombination such as surface passivation.

Open circuit voltage, Voc-

The maximum voltage that can be drawn across a solar cell terminal is known as open circuit voltage. For obtaining Voc, infinite load has to be connected, i.e. the circuit is left open with no current flowing through it. Practically, it could be understood as the potential created by the separated charge carriers on both the sides of junction. Hence, the open circuit voltage depends completely on number of charge carriers generated. Various factors that affect the open circuit voltage can be discussed as following-

Saturation current-As seen from the above equation for Voc ,it depends on light generated current as well as saturation current of diode. From the previous reports, it has been concluded that dependence on I_L is small, while the dependence on Io is quite large.

Recombination – The saturation current or the reverse current of diode has a direct relation with the number of recombination and the type of recombination, hence they also affect the open circuit voltage largely. Voc is maximum at equilibrium where the rate of generation of charges is equal to the rate of recombination.

Built-in potential- Voc depends on built in voltage, Vbi generated by the diffusion of majority carriers after the formation of p-n junction. This can be expressed as the following relation.

$$V_{bI} = Vt \ln\left(\frac{N_A/N_D}{N_V}\right) - \Phi \quad (6)$$

Doping concentration-Voc also depends on the donor and acceptor concentrations. As the donor concentration increases, the Fermi level moves up while when the acceptor concentration increases the Fermi level moves down. In both the cases, built in voltage increases leading to increase in Voc.

Fill factor-

Fill factor is an important parameter which determines the quality of solar cell. The maximum theoretical power is obtained at open circuit voltage and the short circuit current. However, the practical power is obtained at lower values of voltage and current.

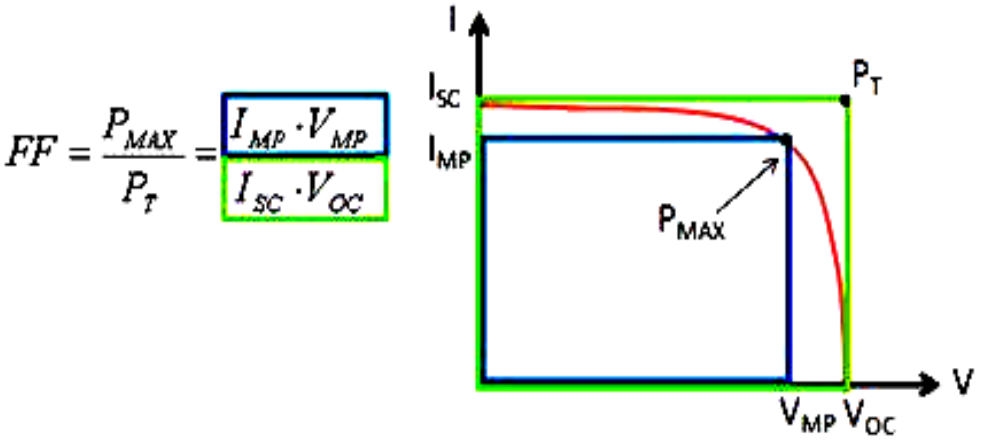

Figure 2.3 Graphical calculation of fill factor [2]

Fill factor (FF) can thus be defined as the ratio of maximum power that can be obtained to the power obtained by the product of open circuit voltage and short circuit current. As shown in figure 2.3. FF primarily depends on the following-

Shunt resistance and series resistance- Fill factor is found to be directly affected by series resistance of solar cell. It is observed that when series resistance is increased by 0.1%, it causes 2.5% decay in the FF value. Since, sheet thickness and resistivity affects series resistance, they also determine the FF values.

Ideality factor-The ideality factor (n), can be derived from slope of current-voltage characteristics. It also depends on quality of junction, the recombination mechanism across the junction and the type of semiconductor being used.

V-I characteristics of solar cell-

The V-I characteristics of a solar cell, as shown in figure 2.4 can be obtained by superimposing the V-I curves in dark with the V-I curve under illumination.

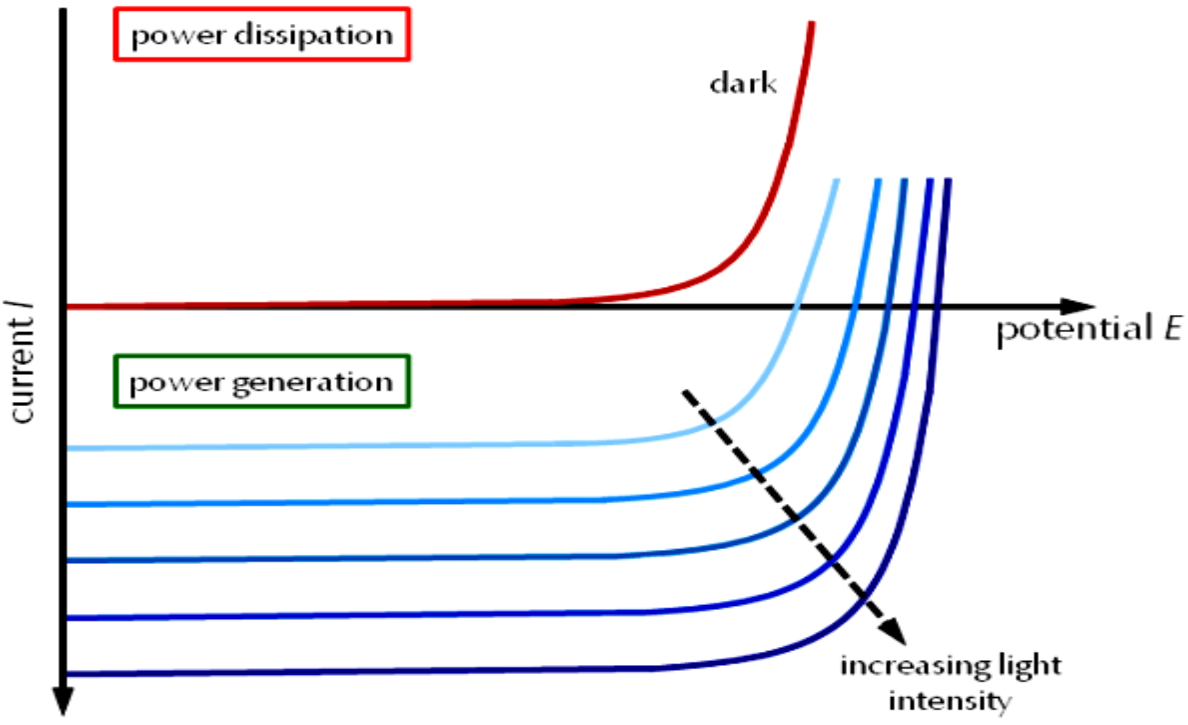

Figure 2.4 V-I characteristics of solar cell [3]

Chapter 3 Types of solar cells

Solar module or the solar photovoltaic array consists of a large number of solar cells in series .As solar cells have been an intense field of research, various types of solar cells are being developed differing in construction and material variability to fulfill desired needs. However, silicon remains one of the most widely used semiconductor material for building a solar cell. The silicon solar cell can be categorized in three fundamental generations as following-

- Crystalline solar cells
- Thin film solar cells
- Heterojunction solar cells

3.1 Crystalline solar cells

Crystalline silicon solar cells are the most common solar cells being used in market .It is because crystalline silicon, also called "solar grade silicon" is stable in nature and they can provide a PCE up to 22%. They could use mono crystalline silicon or multi crystalline silicon depending on the manufacturing process. Their working can be described as following steps-

A semiconductor material can be an electron carrier (n-type) or a hole carrier (p-type).Solar cell is a very large p-n junction diode as shown in Figure 3.1(a) with n-type(phosphorous) having an electron in excess whereas p-type (boron) with a hole in excess.

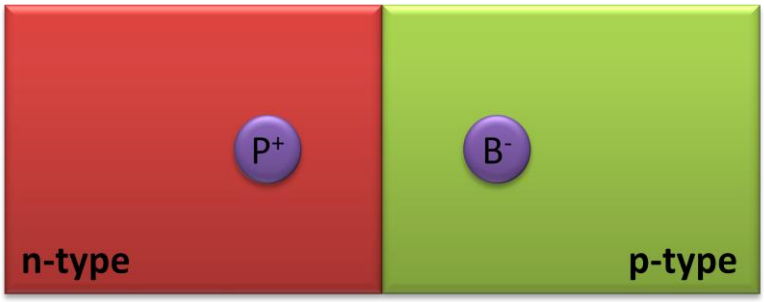

Figure 3.1(a) basic p-n junction diode

The excess electrons on n-side and the excess holes on p-side flows to the opposite side due to concentration gradient as shown in Figure 3.1(b). This leads charged ions behind and the generation of diffusion current in a p-n junction diode in the direction as shown below.

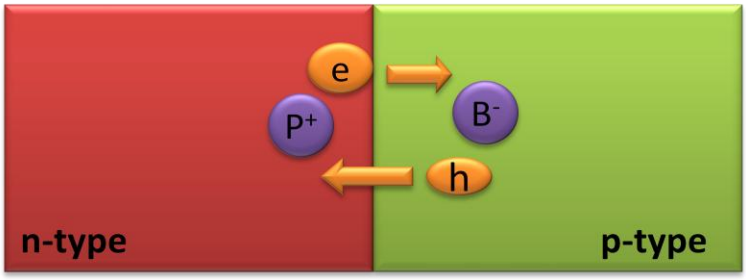

Figure 3.1(b) Diffusion of majority carriers

Due to the diffusion of majority charge carriers ,the ions left behind create a built-in potential as shown in Figure 3.1(c). This electric field supports the drift current(by minority charge carriers), while it opposes the diffusion current(by majority charge carriers due to concentration gradient)

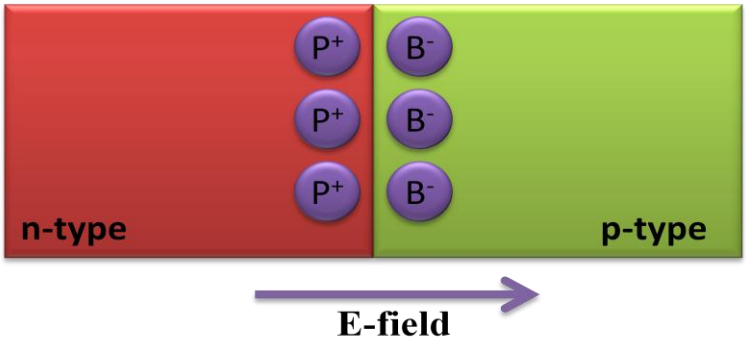

Figure 3.1(c) Formation of depletion layer

Now, when photons (sunlight) with a energy greater than the band gap of material strikes the solar cell, this energy breaks down the covalent bonds deep down the semiconductor and generates free electron-hole pairs.

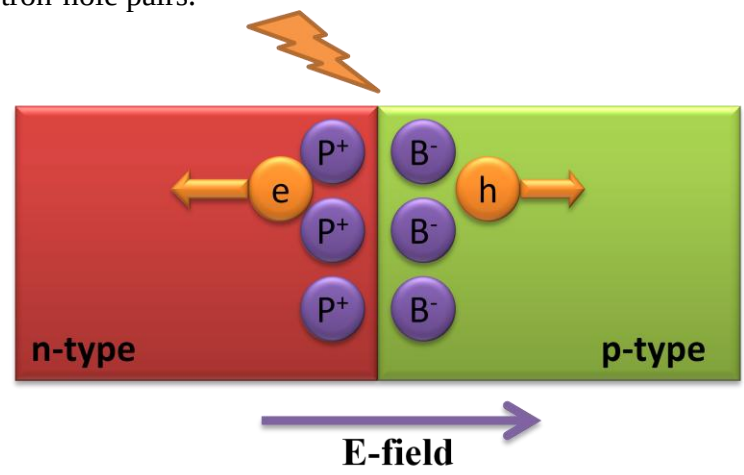

Figure 3.1(d) Generation of EHP

Due to the built in potential, electron and holes get separated at the junction as soon as they reach there as shown in Figure 3.1(d) and move towards opposite electrodes.

But if the energy of photon striking is less than the band gap of absorber material, it is unable to form EHP After the separation of charge carriers, they move to opposite electrodes i.e. electrons move towards n-type electrode where it is a majority charge carrier and photocurrent flows from p to n direction shown as I_{PC} in th figure 3.1(e) which is opposite to the direction of in-built electric field. However due to diffusion of majority carriers, still a small forward current flows through the junction in the direction of electric field. Hence, the total current from the solar cell can be calculated as a difference of forward current (I_{diff}) and the photo generated current.

When the solar cell is short circuited(V=0), the current across the terminals due to generation and collection of light generated carriers is known as short circuit current denoted by I_{SC}. For an ideal solar cell with low loss mechanisms, short circuit current is always equal to photo generated current(I_{PC}).

Whereas, open circuit voltage is the maximum voltage across the terminals when the current is zero (terminals are left open). The open circuit voltage mainly depends on the saturation current of diode which in turn depends on the recombination losses in a cell.

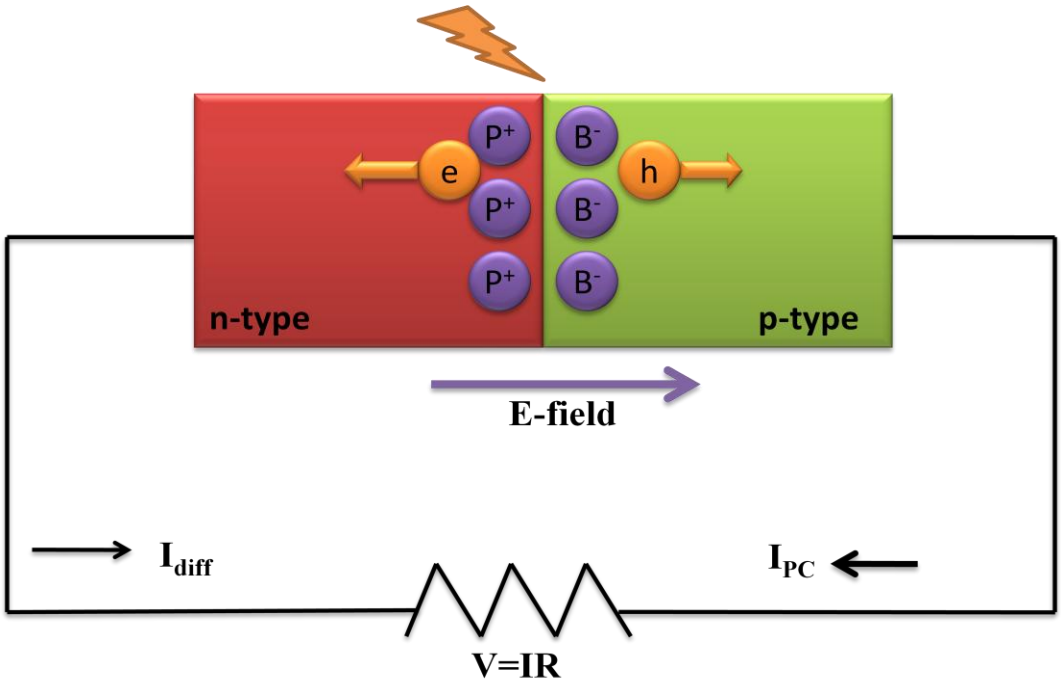

Figure 3.1(e) Flow of photogenerated current along the circuit

3.2 Thin film solar cells-

The second generation of solar cells is known as thin film solar cell. They are made by depositing one or more layers of a photovoltaic material on a substrate. The substrate could be a glass, plastic or a metal while the photovoltaic materials most widely used are cadmium telluride, copper indium gallium diselenide and amorphous thin film silicon instead of crystalline silicon.

In these solar cells, the absorber material thickness varies from a few nanometers (nm) to tens of micrometers (um), much thinner than the first generation crystalline solar cells whose thickness is even more than 200um. Due to the thickness of films, it allows them to be flexible, lower in weight, along with less drag or fiction. But since, thickness of absorber material is directly proportional to the number of absorbed photons, thin film solar cells had limiting efficiencies. However, recently the PCE of these solar cells have been improved to about 21% using CdTe and CIGS as photovoltaic materials. The thin film solar cell consists mainly of 6 layers i.e., transparent conducting layer on the top followed by anti-reflecting coating ,p-type and n-type material ,electrical contact and the substrate. The working of a thin film solar cell is similar as that of a crystalline solar cell.

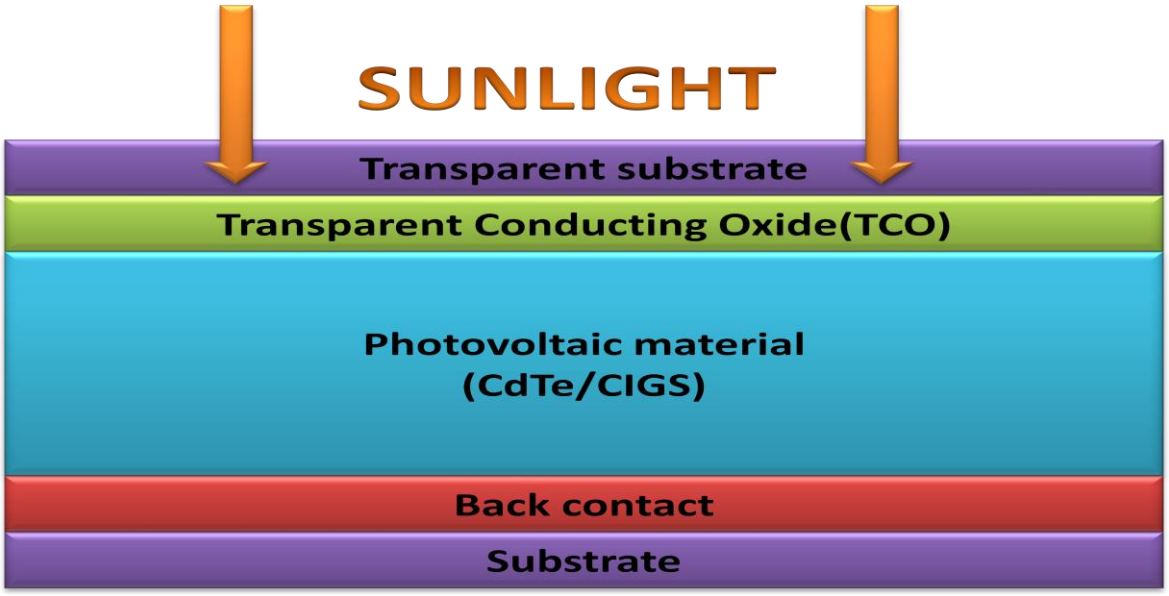

Figure 3.2 Schematic of a thin film solar cell

The transparent conducting film has been used to provide electrical contacts with low resistance, they are desired to have high conductivity and transparency so that they do not block

any incoming radiations from the sun. The schematic of a thin film solar cell is shown in above Figure 3.2 Amorphous silicon is now a days widely used in thin film technology. Unlike CdTe and CIGS, amorphous silicon has advantages of material availability, low toxicity and lesser humidity issues. It requires low processing temperature in synthesis process enabling a large scale production upon low cost substrate material. It has a band gap of 1.7eV which is the optimum value for solar cell absorber material enabling a wide range of radiation through it[3]. Because of this band gap, the solar cell is capable of performing in weak daylight, early mornings or on a cloudy day unlike the conventional crystalline silicon solar cells.

3.3 Pros and cons with single junction cells and thin film homo junction cells-

Single crystalline solar cells uses commercial grade silicon providing very high efficiencies upto 25% . Also, c-Si is abundant, environment friendly and stable in nature thus maintaining high stability of cell, logetivity and easy fabrication. They are highly heat resistant along with very low installation costs. But on the negative side, the initial cost of manufacturing is very high. Since the solar cell output directly relates with the quality of c-Si being used, the silicon has to have purity above 99%. Also, they show fragile and rigid nature as well as low absorption coefficient due to lower band gap.

While the second generation of solar cells, i.e. the thin film solar cells are much more economical than the conventional solar cells. They provide flexibility and are more compatible owing to their low weights. Since amorphous silicon has a optimum band gap for solar cell material, they have a larger absorption coefficient. The main disadvantage with thin film solar cell is their low efficiency which even make us to over look its low cost benefit. Due to their flexible nature, they are not at all easy to install and need to handled carefully.

So, there comes a need for third generation of solar cell which can have the advantage of both the preceding technologies. Solar cell that can have desired efficiencies along with being cost effective and stable.

3.4 Introduction to heterojunction solar cells-

A heterojunction is formed when two dissimilar metals or semiconductors are brought in contact with differing band gaps unlike homo junctions which is formed by same type of

substrate. First successful heterojunction solar cell was introduced by SANYO , Japan in 1992 , named as HIT cell ,which used a-Si:H nd c-Si to form a p-n junction diode[5]. It also used a thin undoped amorphous silicon intrinsic layer between the two semiconductors of less than 20nm.Advantages and features of silicon heterojunction solar cell over the preceding technologies can be pointed as follows. They consist of amorphous silicon layers deposited on crystalline silicon wafer enabling PCE up to 20% at large scale productions. Recombination at the surface due to dangling bonds of a-Si can be reduced by using hydrogenated amorphous silicon for passsivation purpose. Lower recombination rate leads to higher open circuit voltages. Heterojunction uses dissimilar metals, hence they introduce conduction band offset and valence band offset which causes easy separation of both the charge carriers along the junction and lower recombination, thus enhancing Voc. They are economical as they use only a thin layer of c-Si, which accounts for 70% manufacturing cost of solar cells. Also, they are stable and have a long life span.

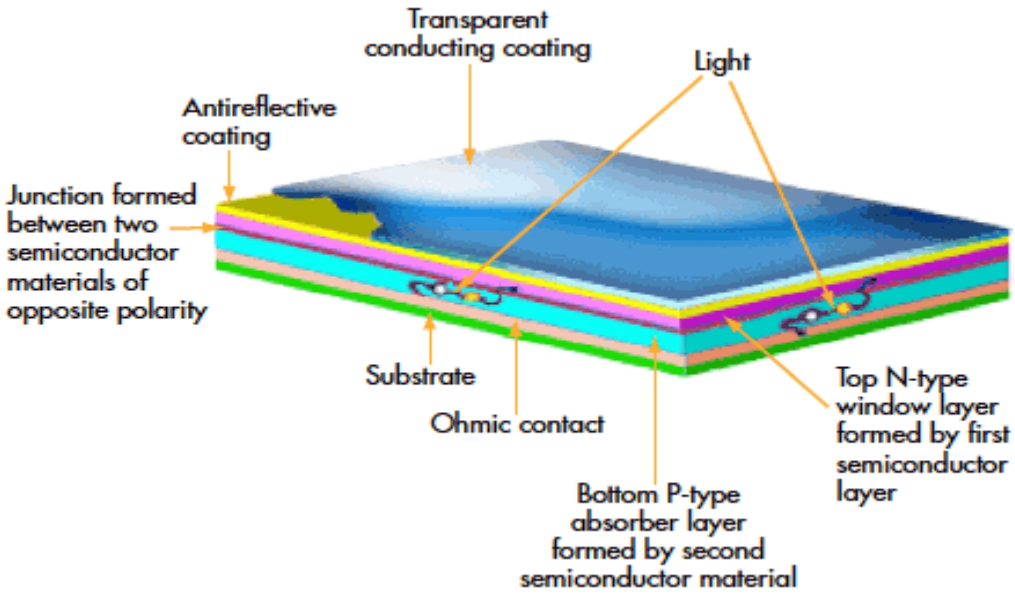

Figure 3.3 Schematic of film solar cell [4]

It has excellent temperature characteristics and considerable output even under diffuse light conditions. Appreciable amount of current can be drawn even in early mornings and cloudy days. High utilization of incident light due to high optical confinement, low absorption loss in transparent conducting oxide and amorphous-silicon and finally the fine patterned electrodes.

Open circuit voltage Voc can be realized over 0.7 volts by using low damage deposition of amorphous silicon on crystalline silicon wafer.

3.5 Types of hetero structures-

When two dissimilar materials are brought in contact, three types of hetero junctions can be formed depending upon the band gaps of both the materials. Due to the difference in band gap and electron affinity, the potential profile of a hetero structure near the junction has discontinuities. This relative alignment of energy bands at the junction of both the materials is known as band offset. Anderson's rule , also known as electron affinity rule is the oldest method used for construction of hetero junctions. According to this rule, when energy band diagrams are being constructed, the vacuum level of both the materials should be aligned at same energy, afterwards the other bands are located with respect to the vacuum taken as reference level. To calculate the conduction band and valence band offsets, electron affinity and band gap for both the material should be known before. Electron affinity can be defined as the energy released from an atom when an electron is added to it in its neutral state. In an energy band diagram, it can be represented as the difference of energy of lower conduction band and vacuum level while the band gap can be represented as energy difference between lower edge of conduction band and upper edge of valence band of a material. Therefore, as per Anderson's rule, the conduction band offset can be calculated as the difference in electron affinities of two materials

$$\nabla Ec = \chi 1 - \chi 2 \qquad (7)$$

where χ_1 and χ_2 are the electron affinities of both the materials. Hetero structures can be categorized in three types depending on the energy band discontinuity they are forming viz, type I, type II and type III as discussed below -

TYPE I (Stagerred gap) hetero structure –

In straddling gap hetero structure, the band gap of one semiconductor is much larger than the second one , such that it completely overlaps the other one in both valence band as well as conduction band i.e, $Ec_1 > Ec_2$ and $Ev_1 > Ev_1$

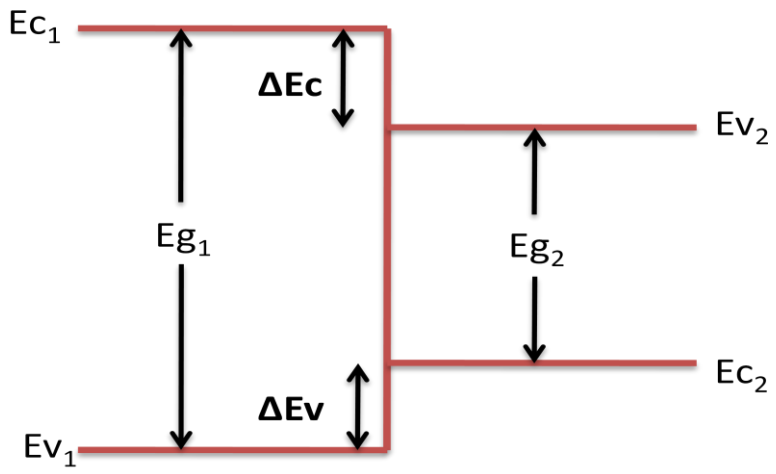

Figure 3.4(a) Stagerred gap heterostructure

Example: this type of hetero structure forms in InAs and AlGaSb

TYPE II (Broken gap) hetero structure –

In this type of hetero structure, the charge carriers electrons and holes are confined completely in both the materials as seen from the energy band diagram below.

Example : observed in InAs/GaSb

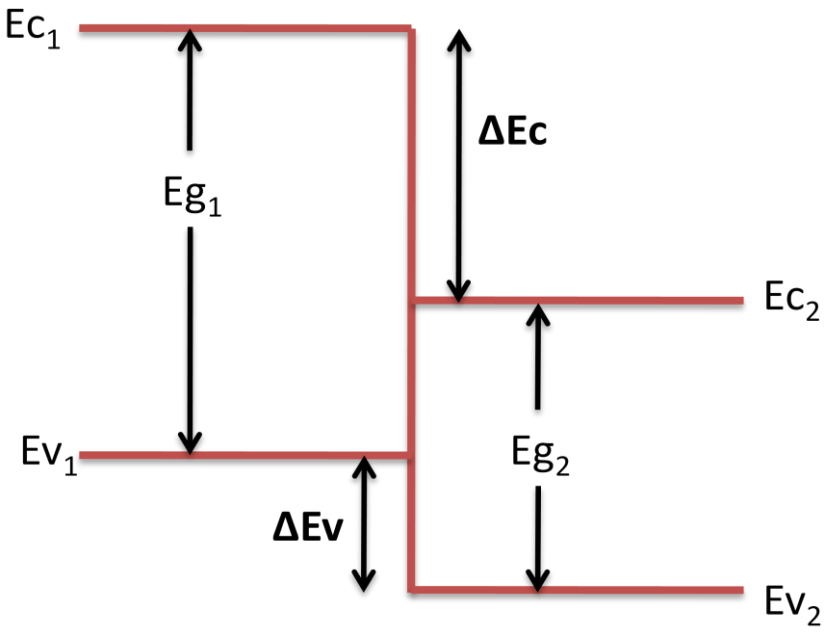

Figure 3.4(b) Broken gap hetero structure

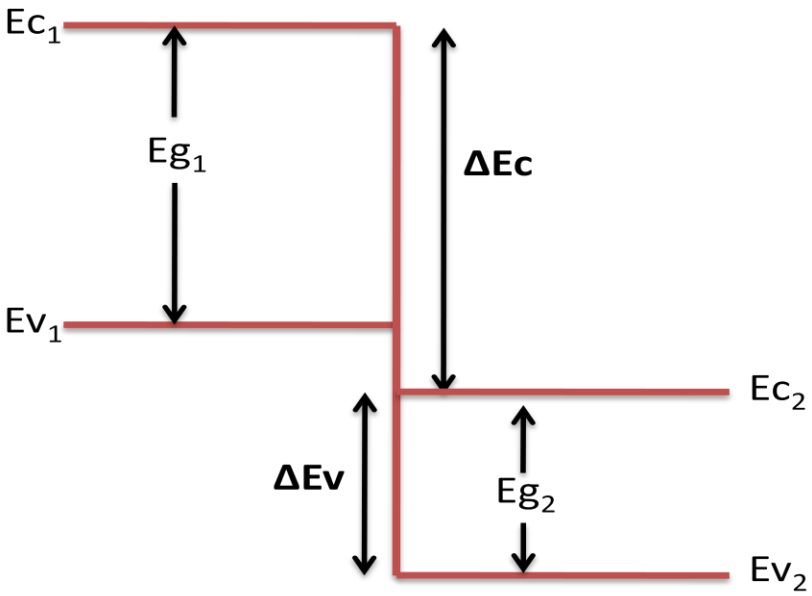

Figure 3.4(c) Straddling gap hetero structure**.**

- **TYPE III (Straddling gap) hetero structure-**

  This is a special kind of hetero structure formed when a semiconductor and a semi metal with inverted bands are brought in contact.

  Example : HgTe and CdTe structures.

3.6 Formation of hetero junction-

The process of generation of charge carriers by photons is similar to that of crystalline solar cells, however instead of homo junction, here we have introduced a heterojunction with conduction and valence band offsets. These two offsets plays the most important role here which enhances solar cell capabilities. When the sunlight strikes the solar cell surface, EHP generation takes place near the junction of cell. Now both the charge carriers under the influence of built-in electric field start moving towards opposite directions. In case of homo junction cells, the some of the charge carriers recombine at the interface and hence this limits the open circuit voltage. However, in case of heterojunction, due to band offsets on both the sides of interface, this unwanted flow of carriers in opposite direction can be minimized to a large extent.

For understanding the working principle of heterojunction solar cell, consider a type II hetero structure as shown below. The energy band diagram can be easily made by using the electron affinity rule.

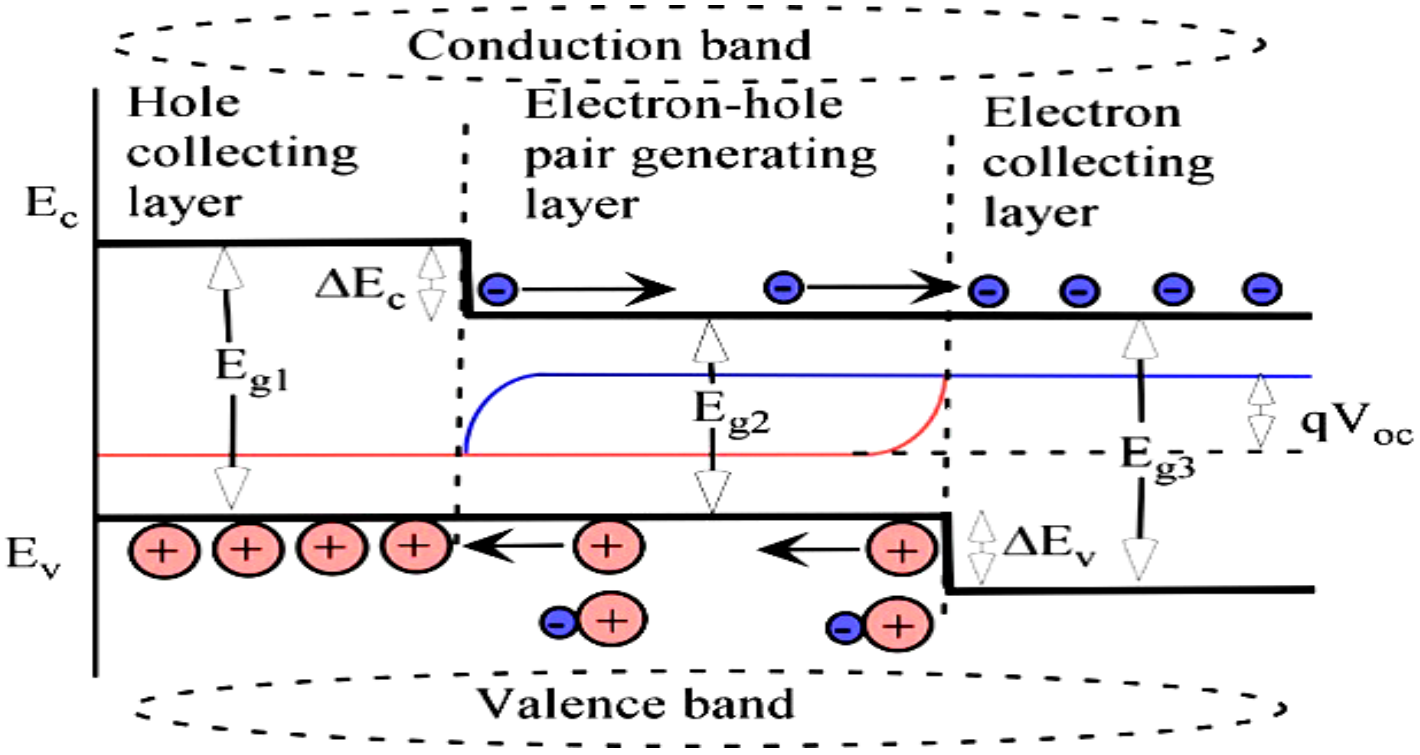

Figure 3.5 Formation of heterojunction and band offsets [5]

The conduction band offset allows the flow of electrons only in one direction towards n-side and restricts the flow towards p-side. Similarly, the valence band offset prevents the flow of holes towards n-side and allows them to move only towards p-side. Larger the offsets on the interface, smaller the number of recombination of charge carriers. Hence ,this model is very effective to get higher values of open circuit voltage and thus leading to higher efficiencies.

3.7 Quasi Fermi level-

Fermi level is defined when equilibrium is achieved between conduction band and valence band (i.e. electrons and holes). The Fermi level shows equilibrium state of semiconductor. However, when this equilibrium is disturbed, due to some external voltage or incidence of light on the semiconductor's surface, the carrier densities get altered in both

conduction band as well as valence band. Hence we use the term quasi Fermi level to describe the electron and hole density separately in conduction band and valence band.

Chapter 4 : Solar cell features

All the solar cells basically consist of following components-

The absorbing layer- This is the most basic requirement for building a solar cell. The absorber layer is the one which absorbs certain portion of wavelengths from the spectrum in form of photons. These photons then are responsible for electron hole pair (EHP) generation .

Top layer- Another semiconductor layer can be added to the cell either at the top or bottom of absorber layer. This layer having different electron affinity and band gap forms a heterojunction with the absorber layer. The main task of introducing this layer is the formation of conduction band and valence band offsets, which facilitate the separation of generated charge carriers.

Electrodes - Once the charge carriers get separated, they move towards the opposite electrode. Electrode serves the task of conveying the photo generated carriers to the external load.

Anti reflection coatings- When the electromagnetic radiation strikes the surface of solar cell, some of it gets absorbed into the cell while the other gets reflected back depending upon the refractive index of material. To minimize this back reflection , anti-reflecting coatings are used at the top of the semiconductor layers.

Back reflectors- Sometimes, the absorber layer is very thin such that it can't absorb all the photons at once. In this situation, the extra energy gets lost by the back surface of the to the atmosphere. To prevent this loss of energy, back reflectors are used which prevent energy releasing from back surface and trapping it inside the cell itself.

Surface passsivation layer- The surface of solar cells faces disruption in crystal lattice due to which it has dangling bonds at the edges. These dangling bonds and other impurities promote recombination known as surface recombination which limits the short circuit current density and thus, PCE to a great extent. Hence, a passivating layer is used at the top surface to reduce the number of dangling bonds and recombination sites. Usually, a thin layer of silicon dioxide ad silicon nitride is used for this purpose at commercial scale production of solar cells.

Transparent conducting films- Transparent conducting electrode (TCE) is optically transparent and very high conducting thin film used in opto-electronic devices. Various oxides are being

used widely under this category because of their abundance and properties. Indium tin oxide with transparency of about 85% and conductivity of $7.2\times 10^{-4}\ \Omega\ \text{cm}^{2}$is the most commonly used TCE material.

For designing various layers and components of solar cells, the materials need to have certain electrical ,optical and physical characteristics for proper working of the module . The basic need is efficient photon to electron conversion and minimizing the losses by parasitic absorption, reflections, recombination by removing defect states or trap states from the solar cell. And finally, conveying the generated carriers to external load.

4.1 Ideal material properties-

To achieve maximum efficiency (PCE), the semiconducting absorber layer should have an optimum band gap in the range o 1-2eV so that it can absorb wide frequencies with high intensities. In order to absorb maximum waves with minimum reflection, the refractive index of absorber layer also plats a very important role.

Another important condition is to that the other functional layers above the absorber layer should be photo-passive, i.e. they should be transparent for the incoming frequencies and have a wider band gap than the absorber material. This will enable the active layer to absorb most of the incoming waves. To avoid reflection losses by other functional layers, they should have a reflection coefficient near to that of the absorber layer. Higher the number of photons absorbed, higher would be the electron-hole pair generation. The solar cell should have minimal recombination at the interface and across the junction to have high photo generated current. Hence, the active semiconducting layer should have low defect density which would avoid recombination. Also, the minority carrier life-time should be very high so that most of the generated carriers could reach the electrodes and contribute to current conduction. In homo junction solar cells, recombination can easily occur at the junction. To overcome this situation, band offsets can be introduced by using another semiconductor with different band gap. The valence band and the conduction band offsets causes holes to move towards p-side only hindering the flow in opposite direction and electrons to flow towards n-side only, thus minimizing the recombination. After generation and separation of charge carriers, they will be collected at the electrodes for which the electrodes should be highly conductive so as to enable

maximum collection. For high conductivity, they should posses high electron or hole mobility and density. The top layer and bottom layer should preferably form ohmic contacts with middle layers whereas it is desired that a strong rectifying junction should be formed at the interface so as to have high conduction band and valence band offsets.

4.2 Types of semiconductor band gap-

Photon to electron takes place differently in direct and indirect band semiconductors as shown in figure 4.1. In a direct band gap semiconductor, the valence band maxima and the conduction band minima occur at same value of momentum. Hence, when a photon is absorbed, it has to undergo only a change in energy for electron emission and maintaining the law of conservation of energy. Whereas, in case of indirect band gap semiconductor, CB minima and VB maxima does not coincide and thus a photon has to undergo both change in the momentum as well as energy.

Therefore, the absorption and conversion of photons is easily facilitated in direct band gap semiconductors instead of indirect ones. Hence if a direct band gap material with high absorption coefficient, is used, only a small quantity could do photo to EHP conversion efficiently.

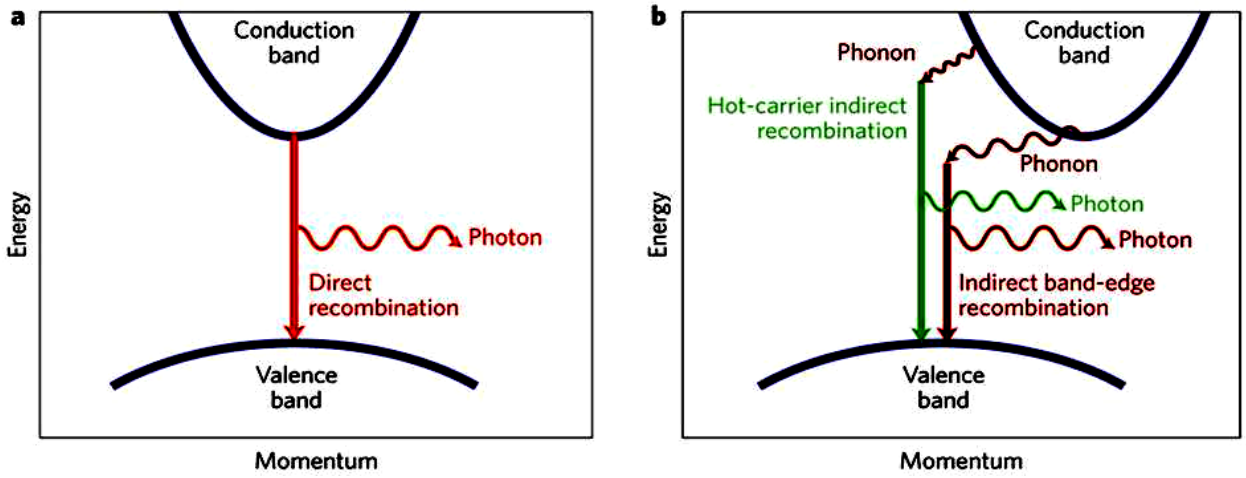

Figure 4.1 Photon to electron conversion in direct and indirect band gap semiconductor [6]

4.3 Sustainability of materials-

In order to be used as solar cell materials at large scale, they should fulfill some technical and economic demands. For using a material at large scale, its raw material cost, production cost and processing (low temperature processing over high temperature and vacuum fabrication) cost should be taken into account. The abundance of material decides the cost of using it, hence if the material is available in abundance, then it would be very economical for large scale production. Furthermore, since the solar cells are being used in all day-today purpose, they should be built of environment friendly material with low maintenance and easy disposal. Silicon being the second most abundant and environment friendly material is thus dominating semiconductor used in photovoltaic industry. However, abundance does not make it cheap, because manufacturing of pure crystalline solar grade silicon is a complex and expensive process Also, oxides are widely used in PV industry owing to their abundance. For economic purpose, small amount of the semiconductor material should be used. Conventional crystalline solar cells uses thick layer of silicon wafer while the thin film and heterojunction solar cells use only a thin layer of crystalline silicon. Highly conductive electrodes also facilitate use of small quantity which reduces the minimization losses also.

4.4 Stability and environment friendly chemicals-

Photovoltaics is a leading technology for sustainable growth. Solar cells are being used everywhere for energy saving purpose, hence they should be made of non toxic materials. Also, the large scale manufacturing process should be environment friendly with minimum harmful by-products. The solar panels used on the top of buildings and houses are vulnerable to environment moisture and impurities which leads to paced up oxidation of all components of solar cell. Therefore, they should be resistant from moisture, air and diffused impurities to have a long life cycle. The exposed layer should also be chemically resistant and stable for which some barrier or encapsulation can be used. Use of certain radioactive and toxic materials such as cadmium ,mercury , is prohibited.

4.5 Metal-semiconductor contacts-

There could be following two types of metal semiconductor contacts depending on the work function and band gaps on both the materials:

Ohmic contact- When two different semiconductors are brought in contact with different band gaps, their energy profile changes at the interface according to electron affinity rule. Ohmic or non rectifying contact is are low resistance stable interface between two semiconductors depending on the barrier height at the interface which in turn depends on the doping of semiconductors. Excellent ohmic contact is formed when the barrier height is minimum, i.e, the difference in band gaps is small. The ohmic contact follows a linear current-voltage characteristic (ohm's law).

Schotkty contact-Schottky, also known as rectifying is formed when the barrier height is large enough to form a depletion layer at the interface. Both the semiconductors have large difference in their work function due to which CB offset and VB offset are formed at the junction. Due to the formation of these offsets, charge separation takes place very efficiently with minimum recombination. Hence, in a solar cell, strong rectifying junction is preferred instead of ohmic contact which can be formed by choosing semiconductors with large difference in work functions.

4.6 Types of recombination models-

Recombination is another important aspect that needs to be considered while modeling a solar cell structure. When there is an empty valence band state, the electron moves to it and removes a hole (vacancy) from there, this process is called electron-hole recombination. Three different mechanisms could take place as shown in figure 4.2 below, depending on the type, various recombination models of electron and hole are discussed as below -

Radiative recombination- This mechanism usually occurs in direct band gap semiconductors .In this case, an electron from conduction band directly recombines with a hole in valence band and thus releasing the energy of process in form of a photon. The photon emitted has the same energy as that of the band gap of semiconductor and is weekly absorbed.

Recombination through defects-This is commonly known as Shockley- read- hall recombination (SRH). It occurs in doped semiconductors and impure materials. In AFORS-HET, we have assumed the solar cell with SRH recombination. The presence of impurity level and defects plays a very important role in determining the carrier lifetime. The defects and impurities give rise to defect levels ,these defect or energy levels do not lie in band gap range, instead they lie in forbidden band of semiconductor. SRH recombination takes place in two steps. Firstly, the electron from the CB will jump to defect energy level in forbidden band. In second step, electron will go down from defect state to the valence band and recombine with a hole.

Auger recombination-This process involves three charge carriers, i.e. two electrons and a hole. It usually occurs in heavy doped semiconductors. Most of the solar cells uses silicon as the absorber layer, where auger recombination is most common mode of recombination.

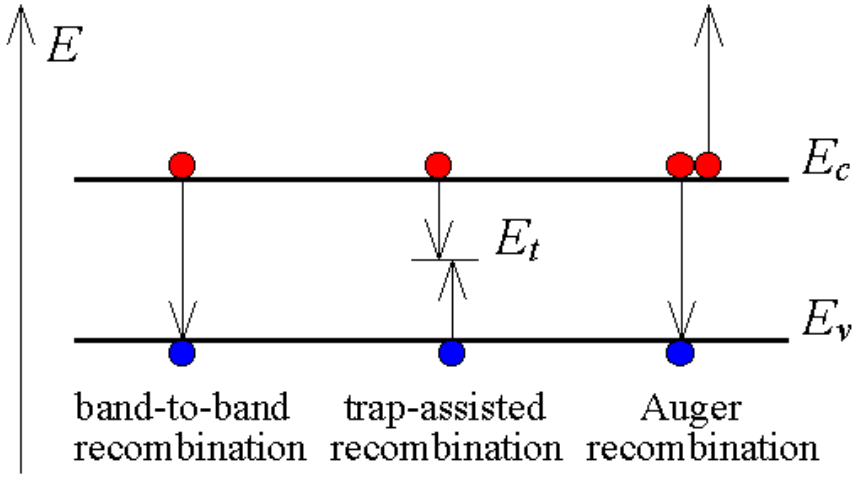

Figure 4.2 Various recombination mechanisms [7]

It is similar to radiative recombination, but after the recombination of electron-hole pair, the recombination energy thermalizes another electron instead of emitting a photon. The auger recombination is directly proportional to doping of semiconductor. For heavily doped semiconductor, the auger lifetime would be shorter.

Chapter 5 : Literature review

5.1 Motivation behind project-

In heterojunction solar cells, the transparent conducting electrode (TCE) is not only responsible for the separation but also the collection of photo generated charge carriers, by forming a barrier at the interface between the electrode and silicon, also serving as anti-reflector. To carry out this task successfully, TCE should have low sheet resistance, for example in ITO, typically order of 20 Ω/sq with 85% optical transmission and mobility as high as > 20 cm^2/Vs [8,9] . Recently, graphene has emerged as a novel transparent conducting electrode (TCE) material owing to its extraordinary properties such as high transparency, sheet resistance as low as 8.8 Ω/sq and carrier mobility exceeding 7350 $cm^2V^{-1}s^{-1}$[10,11]. However, graphene's emergence as TCE material was limited due to low photo responsivity and poor external quantum efficiency, which originate from the zero band gap and low light absorption coefficient [12,13]. These limitations of graphene can be overcome by using atomically thin 2-D transition dichalogenides (TMDs), as they posses relatively large band gap (1-2 eV) and carrier mobility as high as 1800 cm^2/Vs[14,15] . These properties ensure that ultrathin sheet of TMD can be utilized in the TMDs/silicon heterojunction solar cells as a new TCE material. Particularly, WSe_2 is one of them.

In recent advance, carrier mobility as high as 500 cm^2/Vs (in bulk) and 250 cm^2/Vs (in single layer) was reported in WSe_2 [16,17]. This is due to low electron/hole effective mass. It was reported that charge carriers in ultrathin TMDs are weakly screened and their carrier mobility is sensitive to the interfaces on both the ends of the semiconductor which caused variation in mobility. In contrast to the other 2D material, quantum confinement in WSe_2 can be observed by studying the valleys in-charge of electron and hole conduction. As the number of layers reduced, these valleys are raised up/down**.** The effect is only apparent if layer number is lower than three [18]. Furthermore, single layer WSe_2 does not exhibit the gapless nature as well as liner dispersion relation as in graphene in spite of having graphene-like hexagonal lattice structure. This happened due to the lack of inversion symmetry. Recently, p-type behavior of as-grown monolayer WSe_2 with mobility of ~0.2 $cm^2V^{-1}s^{-1}$ and carrier concentration of nearly 1×10^{18} cm^{-3} was confirmed [19]. In further advances possibility of both n-and p-doping in WSe_2

has been demonstrated [20]. Lee et.al reported that by using hydrazine treatment p-type WSe_2 can be converted to n-type with enhanced electron conduction as well as reduced work function [21]. Having such extraordinary properties, to the best of our knowledge experimentally or theoretically no heterojunction solar cell using WSe_2 as a TCE has been reported yet. In this work, we propose n-WSe_2/p-silicon heterojunction solar cell. Since mono or multi layer WSe_2 can be directly deposited on silicon substrate either by using CVD method or vapor phase deposition , this motivates us to optimize the parameters of proposed heterojunction solar cell . Thus, we have simulated the n-WSe_2/p-silicon structure under air mass 1.5 (AM1.5) illuminations with power density of 100 mW/cm^2 using AFORS-HET version 2.5 (Automat For Simulation of Hetero-structures) software. This software uses 1-D semiconductor equations related to Shockley–Reed–Hall statistics solver and Lambert–Beer law based optical model to obtain the optimized parameters. In simulation n-type WeS_2 film is assumed to be 3-D in nature and is taken as cathode and the parameters of both WeS_2 and crystalline silicon (c-Si) layers are optimized in order to achieve highest efficiency of WeS_2/silicon heterojunction solar cells. The present simulation aims to study the independent effects of layer's parameter on the performance of the given solar cell structure and to analyze simulated results. After simulation, we have achieved PCE as high as 13.09 % (100 μm thick p-type silicon).

5.2 Transition metal dichalcogenides-

Transition metal dichalcogenides are most widely studied layered structures due to their extraordinary electrical and optical properties depending on their physical structure. Many 2-dimensional compounds have been explored, among them TMCDs are found to be most stable and high quality 2-D materials. Some of the important properties of TMCDs are listed below-

Physical structure:

They are the compounds formed by transition metals (M) and chalcogens (X) with chemical formulae MX_2. They have been successfully exfoliated to mono layers and characterized. Structure of layered TMCDs is very similar to graphite structure while mono layers are hexagonally ordered films of transition metal stuck between hexagonal films of chalcogens atoms at both sides. The mono layers have reported thickness of the order of 0.6-0.7 nm [22]. They have strong in-plane covalent bonds and weak interlayer van der waals bondings. Due to

these weak van der waal interaction, it is feasible to synthesis mono and bi layer TMCDs by mechanical exfoliation method. The figure 5.1 shows structure of monolayer MoS_2.

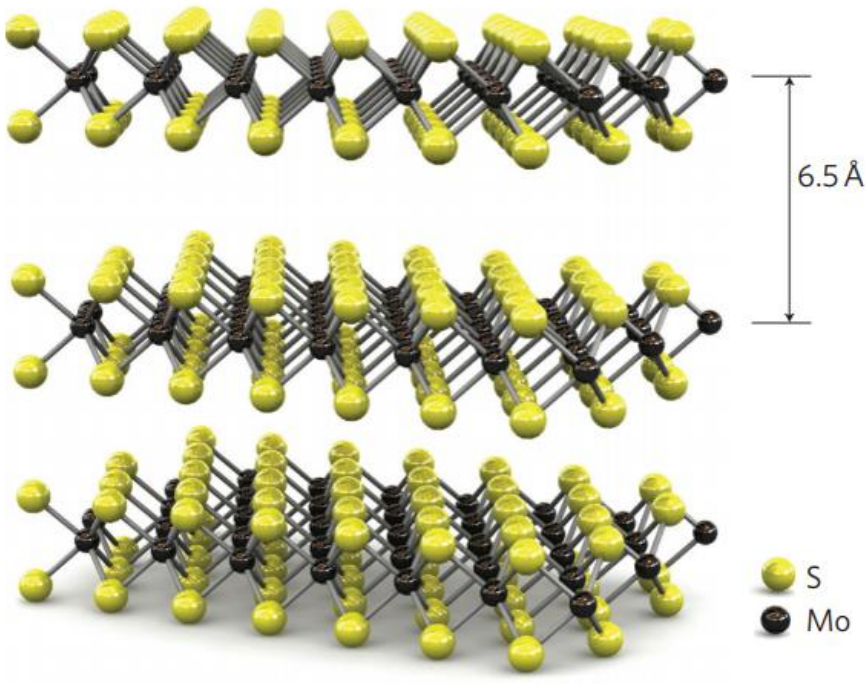

Figure 5.1 Atomic structure of monolayer MoS_2 [23]

Band gap and electrical properties- Graphene due to its zero band gap structure could not be used in opto electronic properties and field effect transistors. However, TMCDs have optimum band gaps in range of 1-2 eV. These band gaps are tunable and depend on physical structure of layered TMCDs. Molybdenum sulphide (MoS_2) and tungsten diselenide(WSe_2) are most widely studied TMCDs as they show transition from indirect band gap to direct band gap after quantum confinement. Bulk MoS_2 is known to have indirect band gap of 1.29eV while monolayer MoS_2 possess direct band gap of 1.8 eV [24]. Similarly WSe2 has bulk indirect band gap of 0.9eV which changes to direct band gap of 1.6eV when exfoliated to monolayer . This band gap transition is not visible in WSe_2 until the layer number is brought below three layers as shown in figure 5.2 below. The figure shows band structures of WSe_2 and MoS_2 bilayers versus monolayers obtained from spectroscopic tools and first principle methods. It can be observed from the figure that monolayers have direct bad gap with higher values.

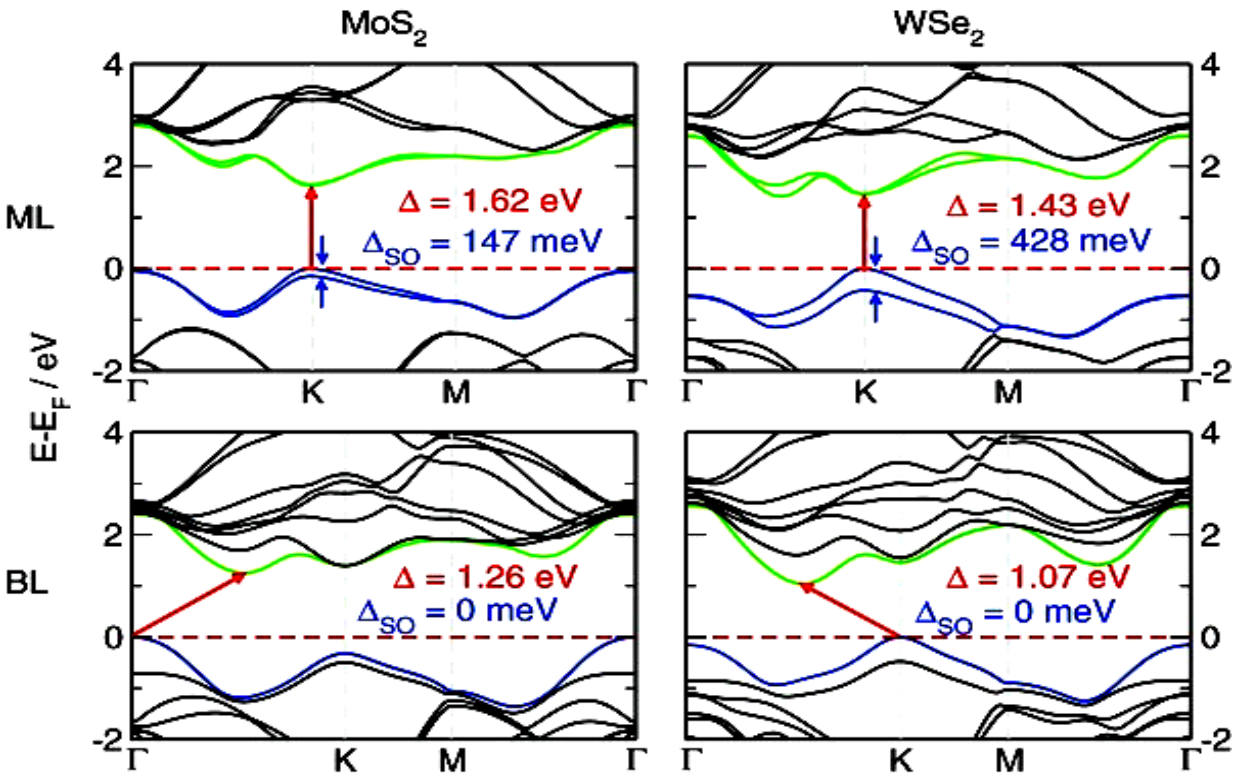

Figure 5.2 Band structures of WSe_2 and MoS_2 bilayers versus monolayers [25]

Conductivity- The conductivity of 2-D TMCDs depends largely on its physical structure. Generally, they behave as stable semiconductors due to the presence of half d-filled orbitals. The electrical properties also vary with the change in chalcogens atom and symmetry of compound also.

Optical properties - With the transition to direct band gap, optical properties of TMCDs such as absorption spectra, emission spectra and photoluminescence. WSe_2 is found to have high transparency and high mobility of about 95%. Other TMCDs also show highly transparent nature such as MoS_2,$MoSe_2$ and Ws_2. Hence Figure 5.3 The spectral variation of reflectance (R) and transmittance (T) with wavelength of WSe_2 single crystal [26] these compounds can be efficiently used in various opto-electronic properties. The figure 5.3 shows transmittance and reflectance curve for WSe_2.

figure 5.3 shows transmittance and reflectance curve for WSe_2.

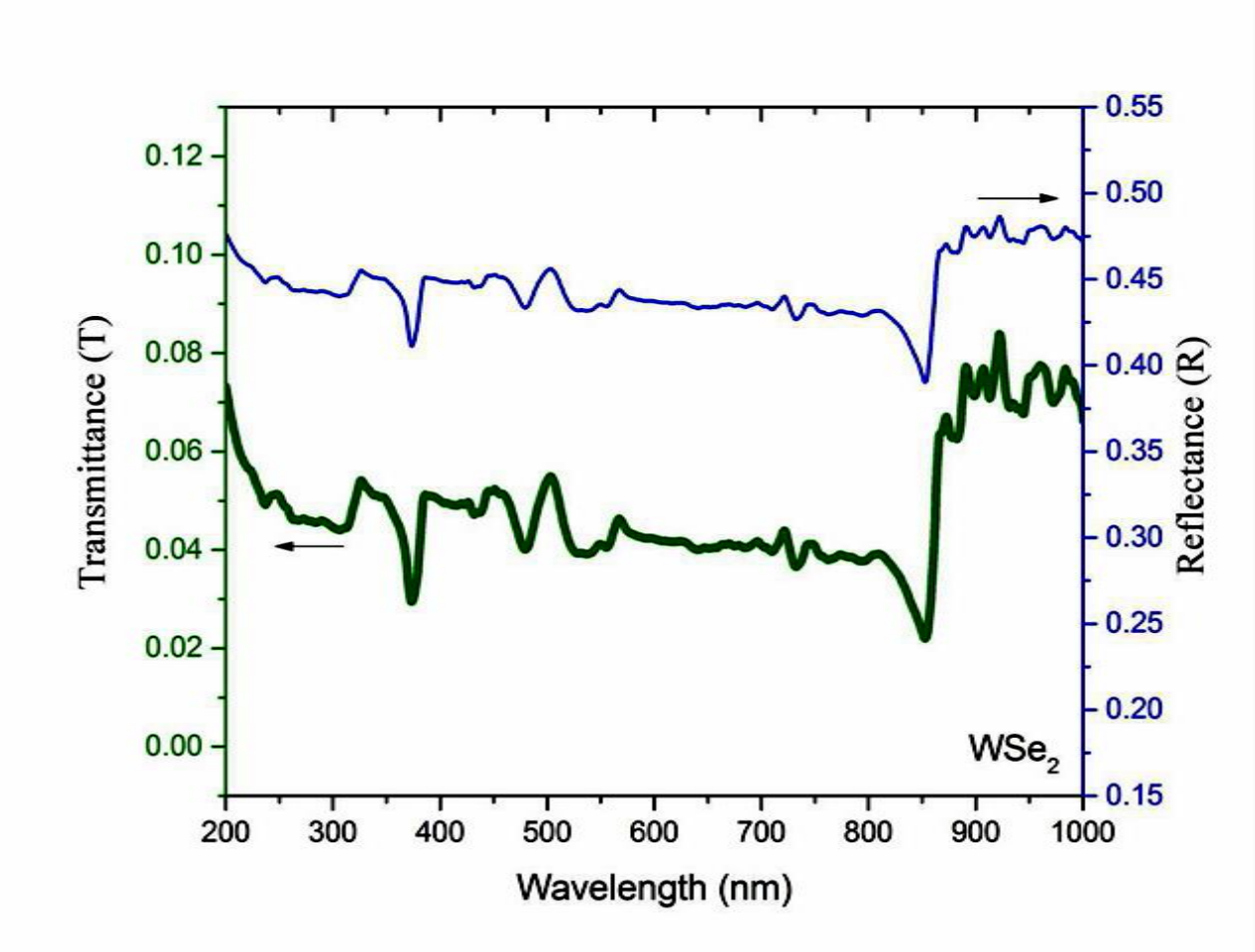

Figure 5.3 Transmittance and reflectance curve for WSe_2[26].

Synthesis-The most common method for synthesis of layered compounds is top-down approach by mechanical and chemical exfoliation depending up on the application where thin films are to be used. Using mechanical exfoliation, one can obtain high purity single crystal films however uniform size is difficult to obtain. Size can be controlled and mono layers can be synthesized using chemical methods with the compromise in purity of films. Other than these, bottom up approaches such as chemical vapour deposition (CVD) and vacuum evaporation can also be used for monolayer synthesis. [27,28]

Applications - They are being widely used in digital electronic devices. To perform as a digital device, it should possess two stable states i.e, "on" state and "off" state. MOSFET (metal oxide semiconductor field effect transistor) can be used for this purpose as it has a high impedance

state and a low impedance state. TMCDs have successfully demonstrated this on/off switching due to their optimum band gaps greater than 1 eV.[29]

Owing to their high mobility values and tunable band gap, they are widely used in field effect transistors. The metal contact electrodes play a vital role in deciding the conductivity of FETs. Low ohmic contacts can be obtained by using metals with very high work function such as indium. Junctions and hetero structures using MoS_2 and WSe_2 have also been proposed. The first proposed model was sandwiched TMCD between 2 graphene layers forming a tunnel field effect transistor. Due to ultrathin nature of TMCD, charge transport takes place via both tunneling and drift-diffusion mechanism. They are also being explored for various opto electronic devices such as photodiode, solar cells and light emitting devices. High transparency, optimum band gaps and high mobility makes them ideal candidate for being used in such devices.

Chapter 6 : Introduction to AFORS HET software-

6.1 Need of simulation-

A simulator is a compilation of hardware and software systems which are used to imitate the performance of some unit or device characteristics. Simulators could in addition be used to investigate and authenticate speculative models which may be excessively complicated to understand from a purely theoretical approach. Hence, simulators provide a essential use in both production and academic world.

Solar cell analyzes via simulation software is very significant because of constant improvement makes cells more multifaceted as more methods , geometrical variables, 3 dimensional effects, and complicated light routes are being introduced. Furthermore, its not viable to propose new cells without simulating them because too many experiments are needed to investigate the design space that would cost very high and is not a practical approach.

Today, there are many simulation software are available for solar cell designing each having some distinct features encompassing various transport mechanisms and other inbuilt phenomenon.

Automat for simulation of heterojunction solar cells (AFORS-HET) is theoretical simulation software for design and analysis of heterojunction solar cells. It can be efficiently used to optimize various design parameters and further characterize them. It is most commonly used to simulate silicon based heterojunction solar cells [30]. The various calculations can be made either in DC mode or AC mode. The various characterization analysis that can be obtained using AFORS-HET in DC mode are V-I characteristics, photoluminescence (PL) , spectral response, internal quantum efficiency(IQE) and external quantum efficiency (EQE). While under AC mode, capacitance-voltage curves, electrolumiscence (PEL), transient luminescence (TR-PEL), impedance and admittance spectroscopy can be obtained.

The main advantage using AFORS-HET is that any arbitrary number of layers can be introduced in the device structure. It can model both one dimensional and two dimensional structures. Advanced version of this software has all possible recombination models and defect states which could be used while designing. The simulation process takes place in two basic

steps [31]. In the majority cases they can be obtained individually. The local generation rate $G(\mathbf{x},t)$ inside the solar cell is determined by optical simulation. It gives the number of surplus carriers (electrons and holes) which are produced per second per unit volume at some value of time and the position inside the semiconductor device of the solar cell as a result of light incorporation. Depending on the optical model preferred for the calculation, effects like external or internal reflections, consistent superposition of the propagating light or light distribution at internal surfaces could be able to measure.

The local carrier densities and the local electric potential within the semiconductor layers of the solar cell are considered for different boundary situations in the electrical simulation. For electrical simulation, the local generation rate obtained from first step serves as input for calculations. Every other internal cell parameter, such as band diagrams, local recombination rates, local cell currents and local phase shifts can then be determined from the local electron and hole densities and from the local potential. The solution for above is found by numerically solving a set of three coupled differential equations i.e, the Poisson equation and the continuity equations for electrons and holes.

In order to simulate a real quantity, the optical and electrical simulations are continually determined while varying a boundary condition of the problem, which is precise to the measurement, like the cell illumination, the external applied cell voltage or the cell current. To assure a numerical simulation with reliable results, a good model calibration, i.e. a comparison of simulation results to a variety of different characterization methods is necessary and the solar cell measured under different operation conditions should be compared to the simulations.

6.2 Defining various parameters-

For the simulation purpose, various material parameters and other properties of solar cell are to be given as input. These parameters can be defined independently according to the proposed solar cell structure. They are discussed as below-

Layer parameters- For each semiconductor film, the width , the electron and hole motilities , the effective valence band density ,conduction band density , the electron and hole thermal velocities , the electron affinity , the relative dielectric constant , the doping profile and the

optical and electrical band gap of the semiconductor has to be defined. Following three different recombination models can be chosen,

(1) Radiative(band to band) recombination
(2) Shockley-Read-Hall(SRH) recombination
(3) Auger recombination

For band to band recombination, the radiative band to band rate constant has to be specified. For Auger recombination process electron and hole auger rate constant should be known. For Shockley-Read-Hall recombination(SRH), the defect density distribution within the band gap of the semiconductor and two capture cross sections have to be specified.

Interface parameters- The electron-hole current transport at the semiconductor-semiconductor interface can be described by three singular interface models;
(1) drift-diffusion without interface defects ("no interface" in AFORS-HET)
(2) drift-diffusion with interface defects ("drift-diffusion" in AFORS-HET)
(3) thermionic emission interface
If model (1) is chosen, no additional interface defects can be specified. Otherwise, an interface defect distribution and two electron/hole interface capture cross sections can be specified. For both models (1) and (2) a interface thickness has to be stated and transport across the semiconductor/ semiconductor interface layer is treated like in the bulk of the semiconductor layers (drift-diffusion approximation), assuming that within the interface layer all semiconductor properties vary linearly from their given values located left and right side of the interface. In model (3) the interface is assumed to be infinitely thin. Interface defects are specified by an interface defect distribution and four capture cross sections , for electron-hole capture from both sides of the interface. Transport across the interface is treated according to the theory of thermionic emission.

Boundary parameters-The semiconductor-metal electrode contact may be metallic or they may be insulating in order to simulate some specific measurement conditions requiring insulator contacts. Four different models can be chosen to specify the interface between metal and semiconductor:

(1) flatband metal-semiconductor contact

(2) insulator contact

(3) Schottky metal-semiconductor contact

(4) metal-insulator-semiconductor contact

If the flatband metal-semiconductor contact is chosen, then there will be no band bending induced within the semiconductor due to the flatband contact. The electron-hole surface recombination velocities of the metallic contact have to be specified. If choosing the Schottky metal/semiconductor contact, an additional work function of the metal contact has to be defined this can give rise to a band bending within the semiconductor. If we opt for the insulator-semiconductor or the metal-insulator-semiconductor contact, interface states connecting the insulator and the semiconductor can be defined, that is an interface defect allocation and interface capture cross sections for electrons and holes has to be specified. In case of the metal-insulator-semiconductor contact an additional interface capacitance has to be specified. The charge in the interface defects can give rise to a band bending within the semiconductor.

Circuit elements- A series resistance, a parallel resistance , a parallel capacitance and in case of a metal/insulator/semiconductor contact also a series capacitance can be specified. If circuit elements are specified, the internal cell voltage and the internal cell current of the semiconductor stack will differ from the external cell voltage *t* and external cell current of the modeled device, which are the measurable quantities.

External parameters- External parameters in AFORS-HET are parameters that are externally applied to the device. These are the temperature of the device, the spectral photon flux and the external cell voltage or the external cell current . The remaining quantity, i.e. the external cell current or the external cell voltage, respectively, will be calculated. In order to simulate a characterization method, some external parameters are varied, while some other parameters which are specific for the measurement, are monitored. For example, in order to simulate the IV

characteristic of a solar cell, the external cell voltage is varied, and the resulting external cell current is monitored.

6.3 Proposed solar cell structure-

The proposed structure for simulation process was made by using n-type tungsten disulphide and p-type silicon layer. For the front contact, indium tin oxide(ITO) is used as transparent conducting oxide which is a n-type degenerate semiconductor with very high work function [32-35]. For back contact, we have used silver (Ag) metal which is one of the highest conducting metal.

Indium tin oxide is known for its large band gap of about 3.8eV, that makes it transparent in visible region and lets the whole light pass through it [36]. It is a highly doped n-type semiconductor, such a high level of doping makes a semiconductor behave as metal. Also,it has high transmittance upto 95% and reported optical conductivity of 10^4 siemens [37]. Similarly, silver too has a very high work function of about 4.26-4.73eV [38].

Both the front and the back contacts are joined to the semiconductors by schottky contacts and are assumed to have a flatband work function for the simulation process. Therefore, the interface (boundary parameters) between the front contact and electron donor layer (n-tungsten disulphide) as well as the back contact and absorber layer would be flat band metal-semiconductor junction. The junction at the interface of both semiconductors would be a normal p-n junction interface. And hence, we will consider the drift-diffusion mechanism for electron transport without interface.

Figure 6.2 shows the heterojunction band diagram. The formation of heterojunction can be explained as, when n-type WSe_2 and p-cSi brought in contact, since $\Phi_{WSe2} < \Phi_{Si}$ electrons were flow from the WSe_2 to p-type silicon in order to occupy lower energy empty states in valence band. This happened because Φ_{WSe2} is lower than of Φ_{Si} and resulted in upward curvature of energy bands because the chemical potential of p-cSi comes in equilibrium with the Fermi level of n-type WSe_2 as shown in Figure 6.2. This in turn creates a region which has depleted the holes and a potential barrier, commonly known as schottkey barrier to reach the interface and then get recombine with an electron. Potential barrier (Φ_{bi}) is given by relation:

$$\Phi_{bi} = \Phi_{Si} - \Phi_{WSe_2} = \chi_{Si} + kT\ln\left(\frac{N_A}{N_V}\right) - \chi_{WSe_2} - kT\ln\left(\frac{N_C}{N_D}\right) \quad (8)$$

Where Φ_{WSe_2}, χ_{WSe_2}, Φ_{Si} and χ_{Si} are the work function and affinity of WSe_2, and work function and affinity of the silicon, respectively. N_D and N_C are the donor ion doping concentration and effective conduction band density of WSe_2, whereas N_A and N_V are acceptor ion doping concentration and the effective valence band density of the p-cSi Under light illumination above the band gap, the photo generated holes and electrons are separated and driven towards the electrode (tungsten diselenide film) and semiconductor layer, respectively, by the built-in electric field. When the solar cell is open-circuited, the separated photo generated electrons and holes will produce an open-circuit voltage Voc. When the solar cell is short-circuited, the extracted photo generated carries will transit through the external circuit, generating a short-circuited current Isc. In this work, the basic structure of tungsten diselenide/silicon heterojunction cell is configured as TCO (ITO)/n-WSe_2/p-cSi/Ag as shown in Figure 6.1. The proposed simulation model uses indium tin oxide as TCO (transparent conducting oxide) in front contact and Ag metal as the back contact. Ag metal passivates silicon back and also avoids the band bending. The other parameters of the contact were given in Table 2. The thickness of WSe_2 tri-layer is fixed at 2.1 nm because value 0.7 nm is the reported for monolayer and then the six parameters i.e. the donor concentration (N_D), band gap (E_g), effective conduction and valance band densities (N_C/N_V), electron affinity (χ), relative permittivity (ε_r) and electron mobility (μ_n) were varied in feasible ranges [39,40,41]. Next, by varying the layer numbers, simulation was performed. Maximum efficiency of 9.055 % has achieved after optimizing n-layer parameters. In second step, we have further optimized parameters p-type crystalline Si (p-cSi) by varying acceptor concentration (N_A), effective conduction and valance band densities (N_C/N_V), the electron affinity (χ) and thickness. Whereas, the other parameters like the relative permittivity (ε_r), electron mobility (μ_n) and band gap (E_g) were fixed at their standard previously reported values [42,43,44]. The various material parameters and their feasible ranges are mentioned in Table 1.

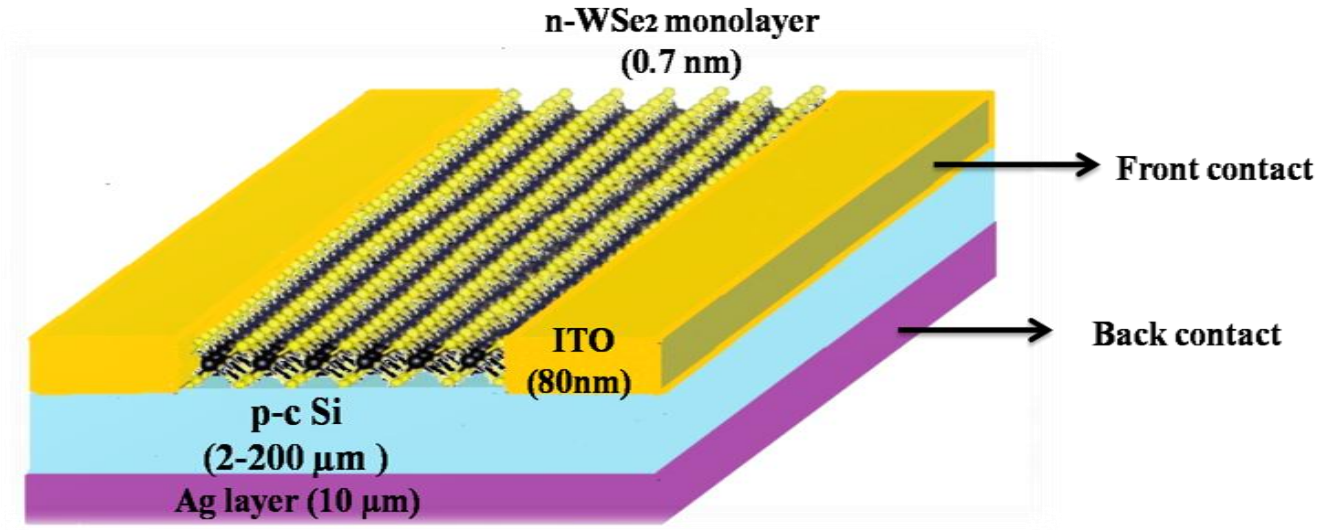

Figure 6.1 Schematic for proposed heterojunction solar cell

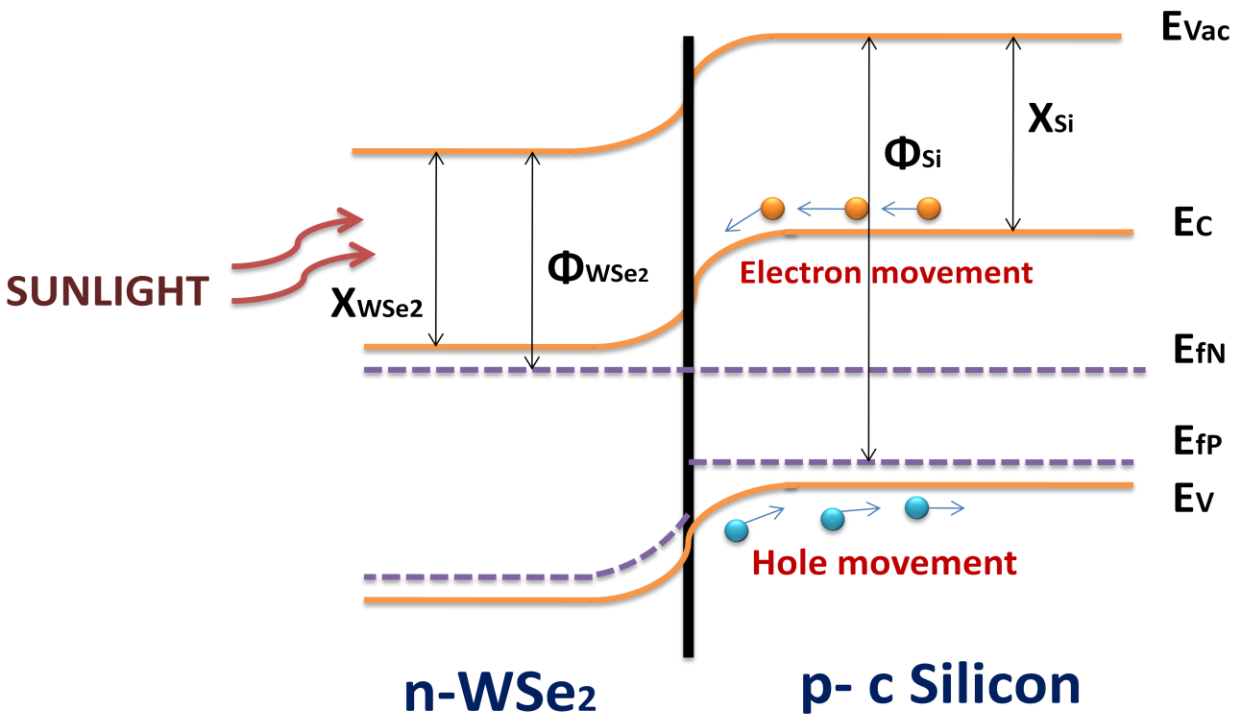

Figure 6.2 Band diagram after the formation of heterojunction at the interface

Table 1. Ranges of various material parameters of tungsten diselenide and p-cSilicon as previously reported.

Input parameters	**n-WSe_2**	**p-cSi**
Relative permittivity, ε_r	6.9-7.5	11
Electron mobility, μ_n (cm^2/V.s)	250	1350
Hole mobility, μ_p (cm^2/V.s)	215	450
Electron affinity, (χ)	3.97-4.15	3.2-4.6
Bandgap , E_g (eV)	0.9-1.6	1.12
Acceptor concentration, N_A (cm^{-3})	0	1×10^{12} -1×10^{21}
Donar concentration, N_D (cm^{-3})	1×10^{07} -1×10^{17}	0
Effective conduction band density, N_c (cm^{-3})	1×10^{17} -1×10^{22}	3×10^{18} -3×10^{25}
Effective valance band density, N_v (cm^{-3})	1×10^{17} -1×10^{22}	3×10^{18} -3×10^{25}
Thermal velocity of electrons (cms^{-1})	1×10^{7}	1×10^{7}
Thermal velocity of holes (cms^{-1})	1×10^{7}	1×10^{7}
Thickness (cm)	7×10^{-8}	2×10^{-4} -200×10^{-4}
Mid bandgap density of states (cm^{-3} eV^{-1})	0	Single acceptor
Switch-over energy (eV)	0	0.56
Auger recombination coefficient for electron (cm^6 s^{-1})	0	0
Auger recombination coefficient for hole (cm^6 s^{-1})	0	0
Direct band-to-band recombination coefficient (cm^3 s^{-1})	0	0

Table 2. Detailed Front contacts and Back contacts characteristics

Contact parameters	**Front contact**	**Back contact**
Width (cm)	8×10^{-6}	0.001
File	ITO.nk	Ag.nk
Metal work function	Yes (flatband)	Yes (flatband)
Absorption loss	ITO.abs	0
External reflection constant	aSicSi_ITO.ref	0
Surface condition	Plane	Plane
Internal reflection constant	0	0

Chapter 7 : Result analysis

7.1 Optimization of n-WSe_2 layer parameters:

1. Optimization of donor concentration

In the proposed simulation, firstly the optimization of donor concentration was done while keeping the other parameters as previously reported values as shown in figure 7.1(a-d).

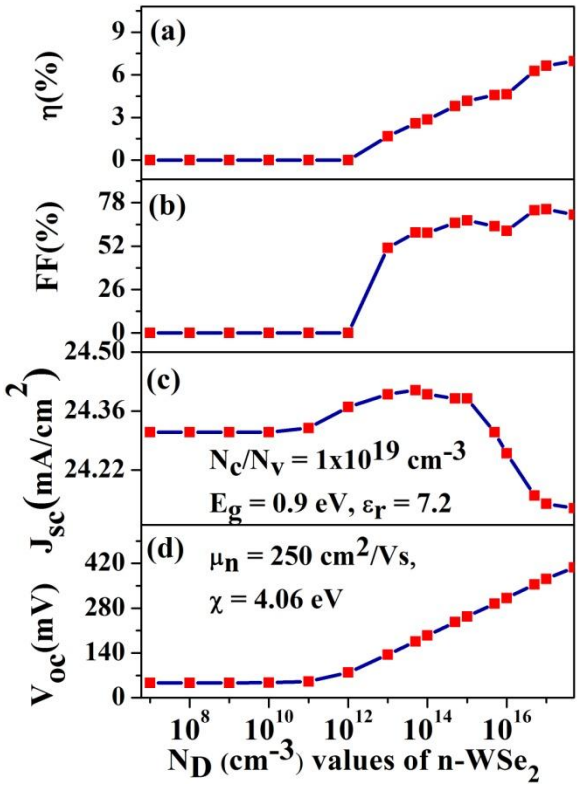

Figure 7.1 (a-d) Optimization of n-type WSe_2 donor concentrations.

As N_D increased from 10^7cm^{-3} to 10^{19}cm^{-3}, there is an upward shift in Fermi level position and level moves closer to conduction band edge, as a result barrier height increases which in turn increases the V_{bi}. As open circuit voltage is linearly dependent on V_{bi} therefore V_{oc} also increases.[45]For low doping concentrations, mobility is almost constant and only be limited by phonon scattering, while at higher N_D mobility decreases due to the scattering with ionized doping atoms. Hence, the current density remains constant initially below 10^{11} cm^{-3}, while at

higher values of N_D it decreases due to decrease in mobility as well as lifetime of carriers [46]. Also, the fill factor of solar cell is determined by its series resistance, shunt resistance as well as ideality factor. Increase in the doping concentration is inversely proportional to the resistivity which consequently increases the fill factor values [47].

The percentage increase in open circuit voltage dominates the percentage decrease in short circuit current and hence the overall efficiency increases to 6.267 % at $N_D = 5 \times 10^{16} cm^{-3}$.

2. Optimization of conduction band and valence band density of states

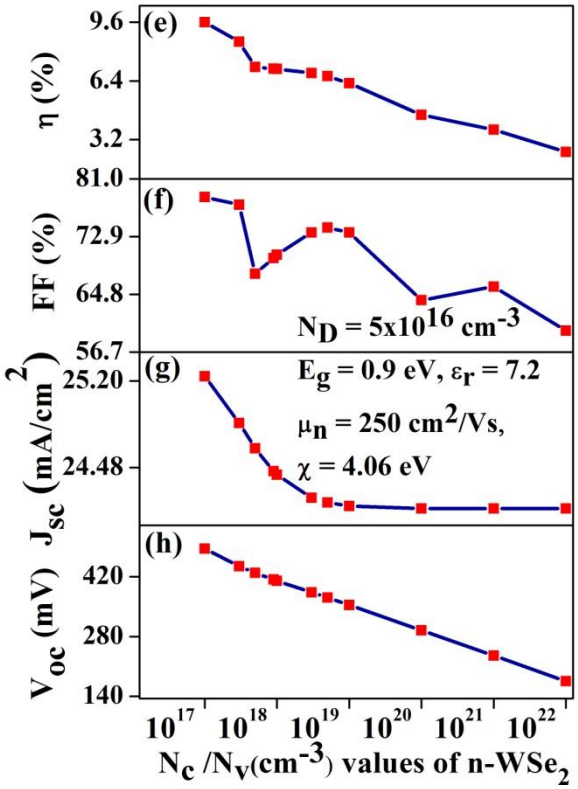

Figure 7.1 (e-h) Optimization of n-type WSe_2 densities of states.

After optimizing N_D to $5\times10^{16} cm^{-3}$, we have optimized the values of N_c/N_v as shown in Figure 7.1(e-h). Initially, Voc decreases sharply along with Jsc as N_c/N_v varied from 10^{17} to $10^{19} cm^{-3}$. Above $10^{19} cm^{-3}$, only V_{OC} decreases and J_{SC} becomes constant to $24.14 mA/cm^2$. The decrease in V_{OC} can be explained by taking in account of equation (8) which shows that conduction band and valence band state density has an inverse relationship with V_{OC}. Also, the

equilibrium concentration of electrons and holes depends on the density of states. The change in this equilibrium condition imbalanced the rate of generation and recombination. This rate is same at equilibrium. If $n_o . p_0 = n_i^2$ where $n_o \; and \; p_0$ are electron and hole concentration at equilibrium and n_i being intrinsic concentration which is directly affected by N_c/N_v, then more recombination occurred [48,49]. This led to reduction in J_{SC}. Due to reduction in both V_{OC} and J_{SC}, efficiency reduces from 9.609% to 2.34% at $N_C/N_V = 10^{22}\ cm^{-3}$. Hence, we have optimized at N_C/N_V value to $5\times10^{17}\ cm^{-3}$.

4. Optimization of n-WSe_2 bandgap

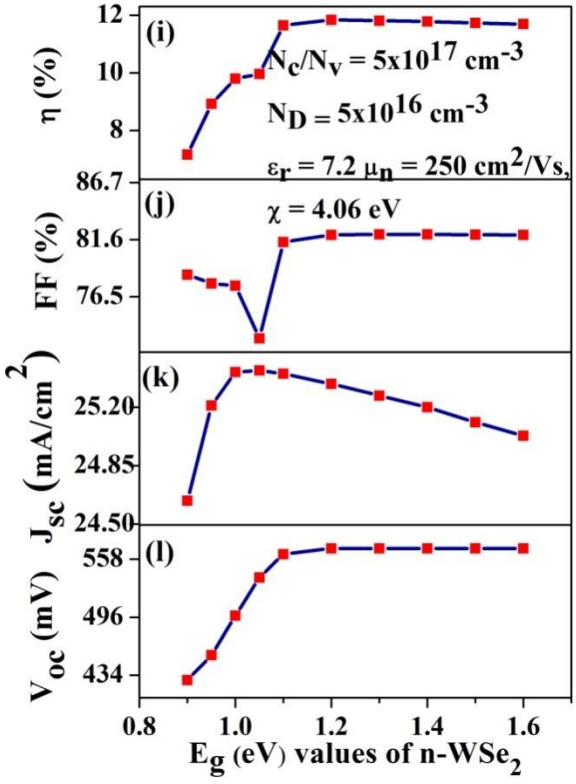

Figure 7.1 (i-l) Optimization of n-type WSe_2 band gap

It was reported that Bulk WSe_2 has indirect band gap of 0.9eV, while monolayer WSe_2 has direct band gap of about 1.6eV [50].So**,** as layer number reduces, band gap enhances. But, band transition (indirect to direct) only observed if layer number is below 3, i.e. trilayer is considered as bulk and quantum confinement can only occur in single or double layer. The same effect could be directly seen while optimizing the band gap, as shown in Figs. 7.1(i-l). As band

gap increases from 0.9 eV to 1.2 eV, there is a sharp increase in device performance because when the band gap is small and indirect in nature, some of the frequencies of photon are hindered. Higher E_g reduces n_i exponentially, and hence V_{OC} increases linearly with band gap [50]. On the other hand, as band gap increases to 1.3eV and above, it becomes a window for all incoming photon and both efficiency as well as J_{SC} increase. On further increasing of the band gap the η becomes constant at 11.71 %. This is due to the pass the maximum of photonic waves.. It was also observed that J_{SC} decreases above 1.2eV. This is because of large photon absorption at low E_g and leads to maximal J_{SC}.

5. Optimization of n-WSe_2 electron affinity

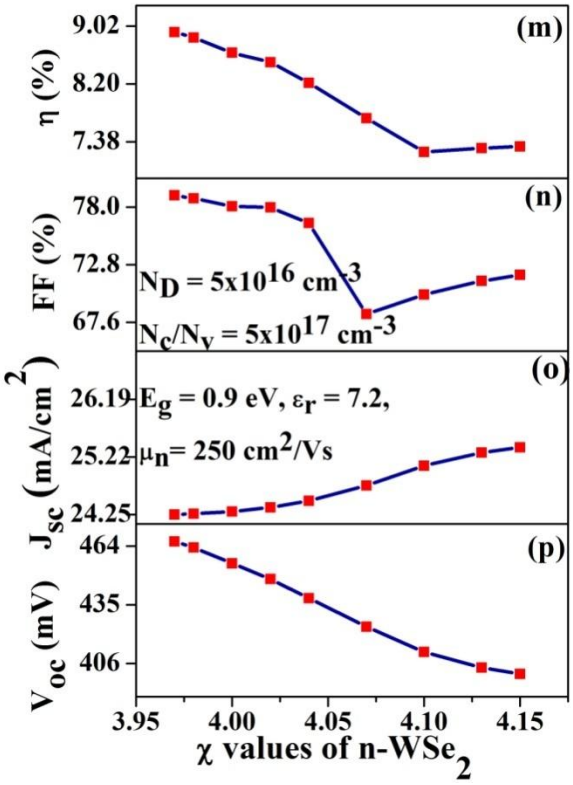

Fig. 7.1 (m-p) Optimization of n-type WSe_2 electron affinity value.

While optimizing χ_{WSe_2}, as shown in Figures 7.1 (m-p), we have observed that V_{OC} decreases from 472.7 eV to 400.8 eV whereas J_{SC} increases slightly. These changes can be understood, as χ_{WSe_2} increases conduction band moves downward and facilitates more EHP generation and more carriers flow across the load, as a consequence J_{SC} increases from 24.64

mA/cm^2 to 25.03 mA/cm^2. Also, the possible decrease in V_{OC} can be observed by equation (1), in which Φ_{bi} decrease as Φ_{WSe_2} increases which in turn V_{OC} decreases. Although, percentage decrement in V_{OC} is high in compare to increment in J_{SC}, as seen in Figs. 7 (m-p), hence efficiency is also reduced to 7.311% at χ_{WSe_2} = 4.15eV. χ_{WSe_2} is optimized to 3.95 eV.

5. Optimization of n-WSe_2 mobility-

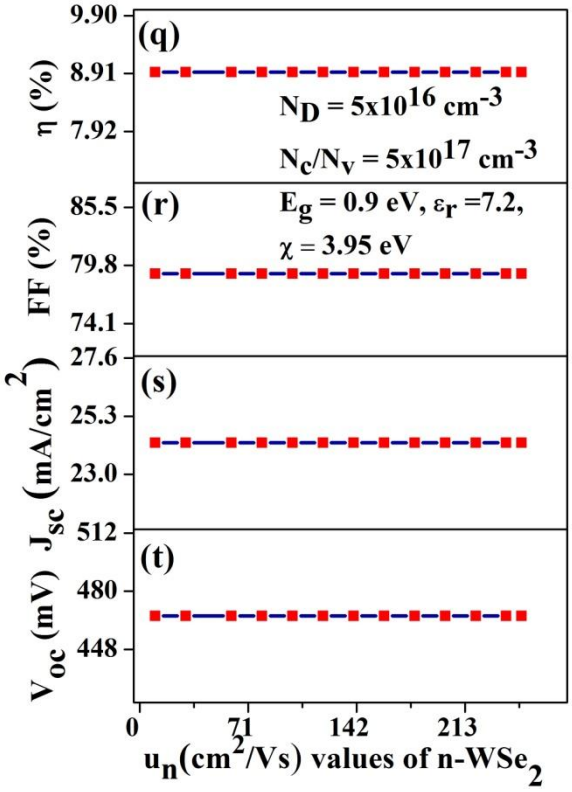

Figure 7.1(q-t) Optimization of n-type WSe_2 mobility

Relative permittivity (ε_r) and electron mobility (μ_n) were also analyzed and found to be unaffected, as shown in Figs. 7.1(q-t). Possible reason for no change in solar cell performance with variation in mobility, might be that the total current in the solar cell is the sum of both photogenerated current as well as dark current. And the power efficiency is limited due to recombination of carriers. For organic solar cells, it was reported that near the short circuit conditions, as the mobility increases the photo generated carrier recombination decreases. While near the open circuited conditions, with the increase in mobility, the dark carrier recombination

increases [51]. Hence these two opposite effects balance each other and the performance parameters of cell remain constant over a range of mobility.

6. Variation with layer number of n-WSe_2

In order to further analyze that in the proposed solar cell whether WSe_2 is only functioning as a transparent conducting layer or actively contributing in photogeneration process too, we have varied layer numbers from 3 to 40. Resulted cell performance parameters have shown in Figure 7.1(y-bb). We found that J_{SC}, FF, V_{OC} and η change as layer numbers increases. As the layer numbers increases, mobility is enhanced [52].

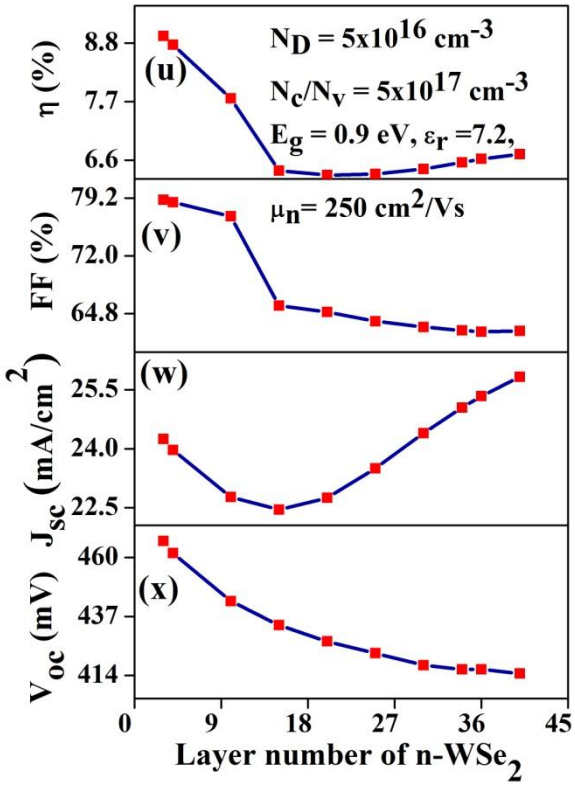

Figure 7.1(u-x) Optimization of n-type WSe_2 layer number

With the increase in mobility, surface recombination became higher which decreased V_{OC} [53]. The same effect may also be the reason for low J_{SC}. Another reason for the decrease in J_{SC} might be due to the increase of optical absorption in WSe_2 which do not contribute to J_{SC}. Hence

lesser number of photons will reach to silicon and results in less photo generated carriers as a consequence J_{SC} decreases. But later, J_{SC} increases which may be due to the fact that increase of layer number reduced sheet resistance which in turn improves efficiency as well as J_{SC}. Also, decrease in fill factor is observed because fill factor is directly affected by series resistance of solar cell **.** So, the overall efficiency decreases with increasing of layer number up to 32 and then slightly improves. After optimizing all parameters of n-type Wse_2 layer, the maximum efficiency of 9.055 % has been achieved.

7.2 Optimization of p-Si_2 layer parameters:

1. Acceptor concentration-

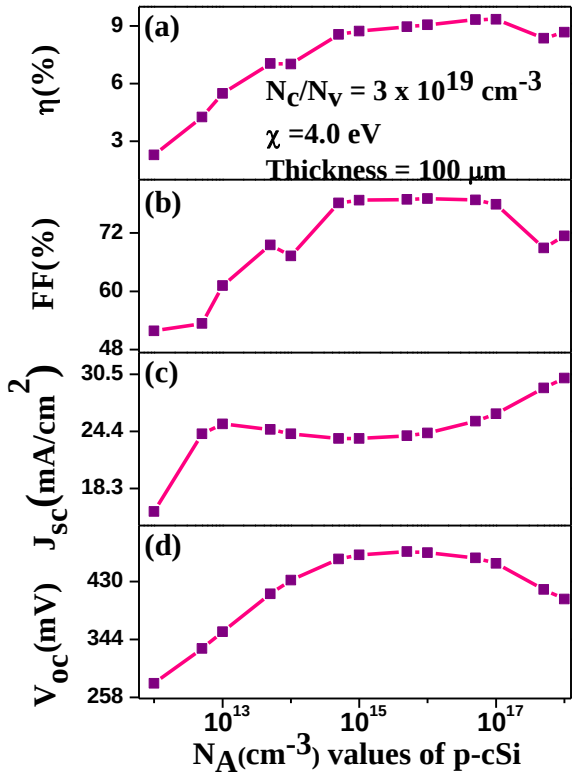

Figure 7.2 (a-d) Optimization of p-type silicon acceptor concentration

In order to further improve the efficiency, parameters of p-type silicon layer has been optimized while parameters of n-WSe_2 are fixed as the optimized ones. When the acceptor concentration (N_A) has increased from 10^{12} cm^{-3}, χ_{Si} decreases, in turn V_{OC} decreases as shown in Figure 7.2 (a-d). η is found to be increased at high doping levels in Si layer. When N_A

increases, Fermi level starts moving down and the acceptor band widens and starts overlapping the valence band. This increases the barrier height (SBH), consequently V_{bi} and as a results V_{OC} enhance. As it is clear from equation (8) that the V_{bi} is directly proportional to N_A which in turn affects V_{OC}. It is observed that V_{OC} increase from 278.9 mV to 457 mV at N_A of 10^{17} cm^{-3}. Under high doping conditions, the minority carrier lifetime increased whereas both surface recombination as well as SRH recombination are minimized. This high doping of silicon absorber layer makes it act as a Back Surface Field (BSF) layer **.** As a result, J_{sc} is increased and consequently η is increased to 9.349 % at optimized N_A (1×10^{17} cm^{-3}).

2. N_C/N_V and electron affinity

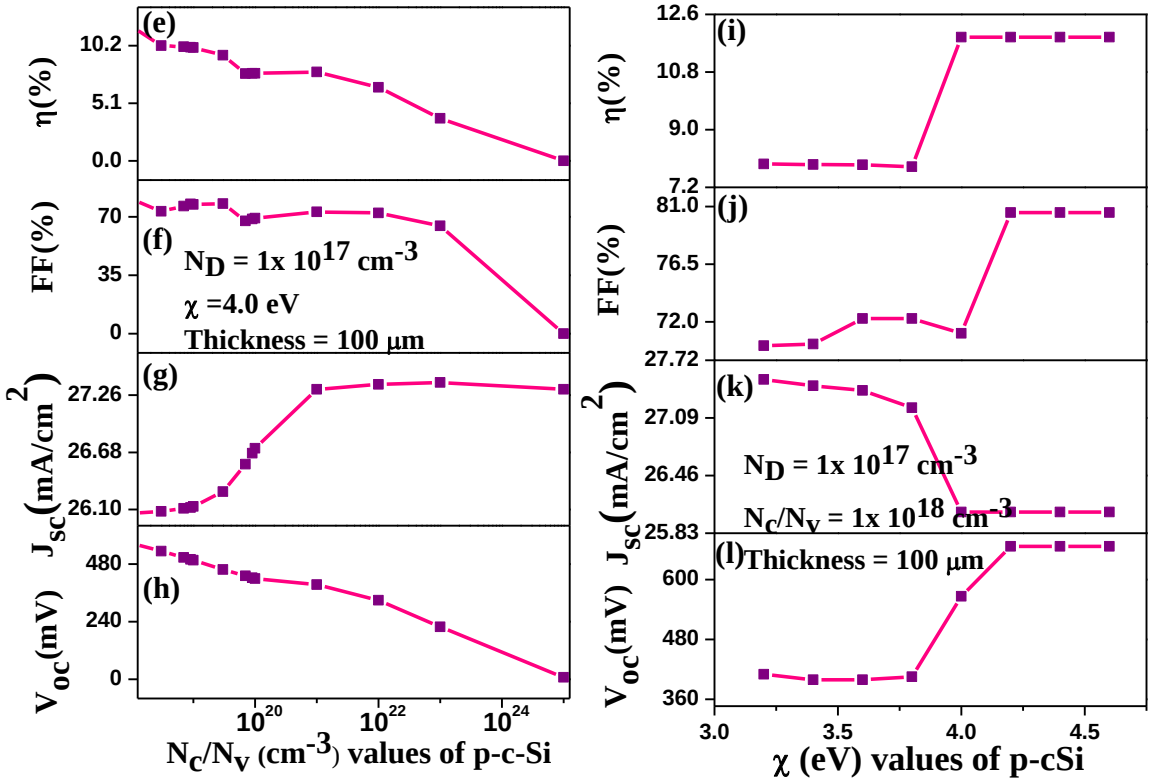

Figure 7.2(e-h) Optimization of p-type silicon density of states and electron affinity(i-l).

After optimizing N_A**,** N_C/N_V was optimized in range of 1×10^{18} to 1×10^{25} cm^{-3}, a liner decrease in V_{OC} was observed. This might be explained as V_{bi} decreased with increase of N_C/N_V and V_{OC} was also decreased from 566.4 mV to 8.549 mV at N_C/N_V 10^{25} cm^{-3} and the overall η decreased with similar rate. However, J_{SC} is slightly increased from 26.06 mA/cm^2 to 27.32

mA/cm^2 with N_C/N_V. This may be due to less recombination across the interface. χ_{Si} has been optimized and found to be 4 eV, as shown in Figures. 7.2(i-l).

3 . Thickness

The most important parameter in determining efficiency of cell is the thickness of absorber layer. To study the effect of thickness variation, we have varied the thickness of p-cSi from 50 µm to 600 µm. We have noticed an appreciable effect in all the parameters [54]. As the thickness increases, more number of photons absorbs and results in large EHP and as a consequence J_{SC} as well as other parameters increase.

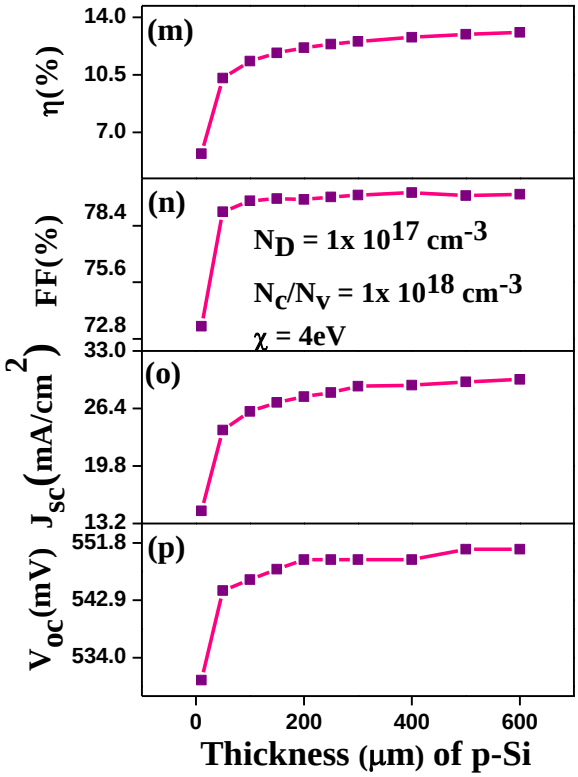

Figure 7.2(m-p): Optimization of p-type silicon thickness

But while optimizing thickness, diffusion length of generated carriers has to be taken in account along with absorbance coefficient. When thickness of Si increases, probability of minority carrier to reach either the depletion region or the back surface of Si layer reduced. Hence recombination in the Si layer might occur as a consequence J_{SC} decreases. As thickness is

increased from 100 μm to 600 μm, J_{SC} increases from 25.34 mA/cm^2 to 29.72 mA/cm^2. Maximum efficiency 13.09 % has been achieved.

4. Layer number of WSe_2 -

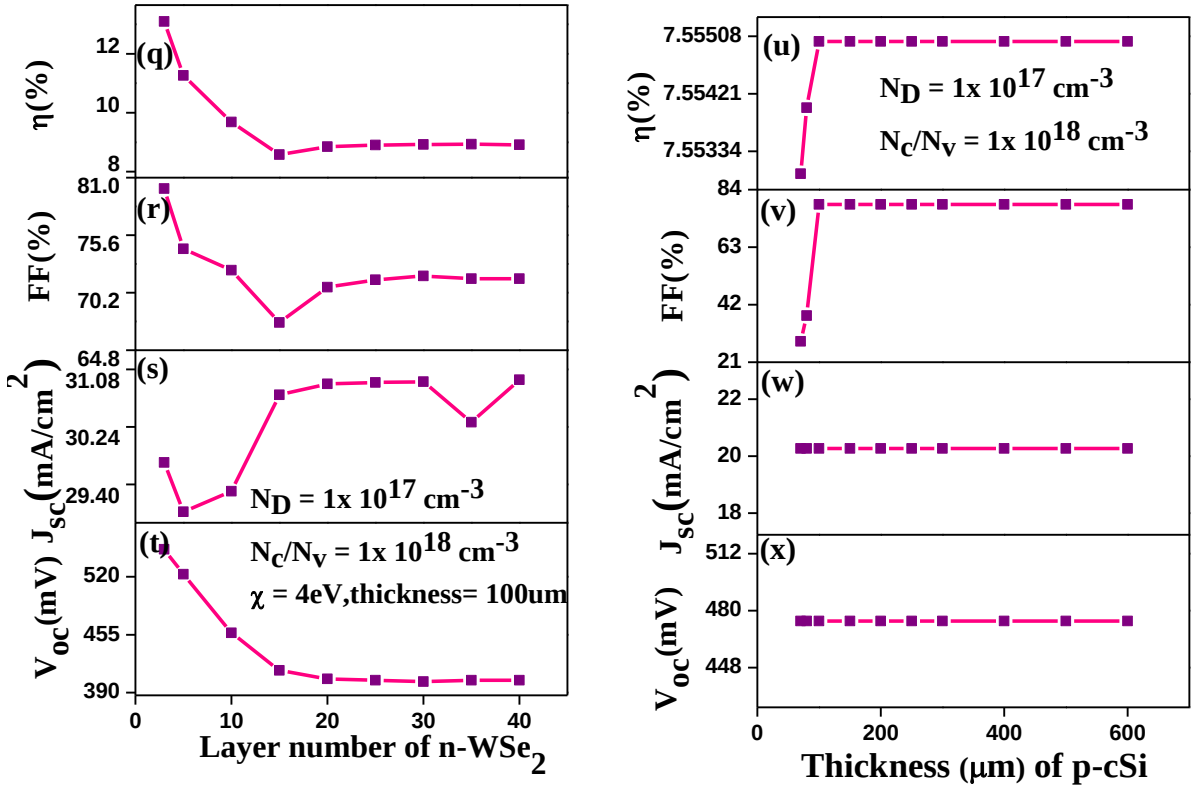

Figure 7.2 (q-x) Optimization of layer number of n-WSe_2 and thickness and thickness of commercial silicon parameters for solar cell output parameters.

After optimizing the parameters of Si layer, cell performance was further analyzed by varying layer number of n-WSe_2, as shown in Figure 7.2 (q-t). η was reduced to 8.584 % as layer number increased and then reached to constant value of 8.914 %. After optimizing the parameters of n-WSe_2 layer, simulation was further performed considering the parameters of standard commercial available silicon as shown in Figs.3 (u-x). η was found to be first increased and then becomes constant if Si thickness was above 50 μm. The maximum value of η for commercial silicon comes out to be 7.555 %. Later, simulation was further carried out by varying both the back contact and front contact. We have simulated the cell by changing the front contact

from ITO to aluminum (n=1.0972, k=6.7943) and the back contact from silver to chromium/silicon (n=3.0504, k=4.2504) as used by Tsai *et al.*, and lower work function material like Titanium (n=1.906, k=3.0606). No change in the simulated results was observed by doing so. Later, simulation was further carried out by varying both the back contact and front contact. We have simulated the cell by changing the front contact from ITO to aluminum (n=1.0972, k=6.7943) and back contact from silver to chromium/silicon (n=3.0504, k=4.2504) as used by Tsai et al.,[12] and lower work function material like Titanium (n=1.906, k=3.0606). No change in the simulated results was observed by doing so.

7.3 Quantum efficiency, spectral response and temperature dependence

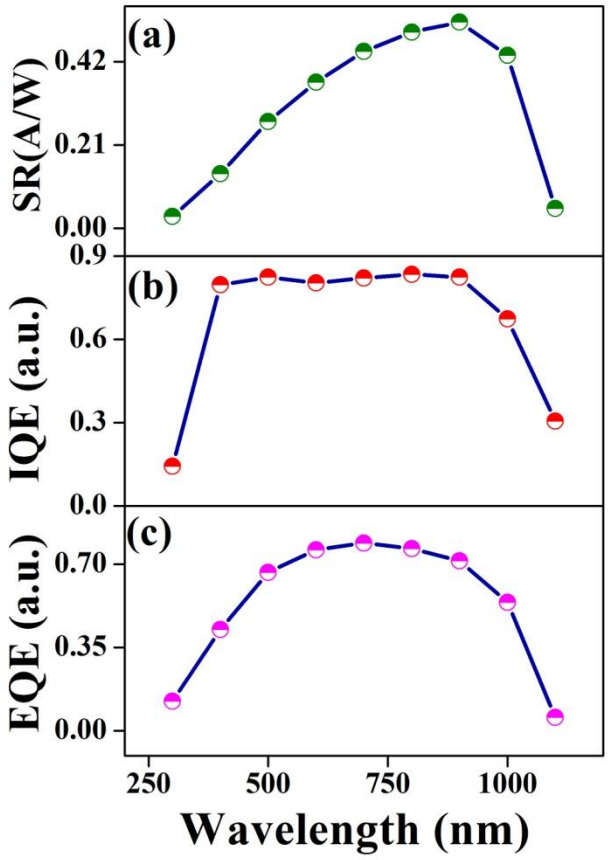

Figure 7.3 (a) Spectral response (b) Internal quantum efficiency (IQE) (c) External quantum efficiency (EQE) of the WSe_2-pcSi optimized solar cell at PCE 13.09 %

The internal quantum efficiency (IQE) is always either high or equal to the external quantum efficiency (EQE). This is due to recombination at the interface. The wavelength dependent characteristics IQE, EQE and spectral response (SR) for the optimized simulated solar cell is shown in Figs. 7.3 (a-c). IQE and EQE have showed quite a similar response with wavelength. EQE and IQE started with a value of about 0.12 and 0.14 at 300 nm and increased to 0.78 and 0.83 respectively in the wavelength range of 300-800 nm. After 800 nm, both are reduced exponentially and become zero at 1100 nm. SR is found to be 0.03 at 300 nm and then increased to 0.51 at 900 nm. Further the SR linearly decreases at higher wavelengths. This is happened due to the inability of semiconductor to absorb photons with energies less than the semiconductor band gap [55].

For analyzing solar cell response under various temperature fluctuation, simulation was performed for best optimized cell in a given temperature range of 200 - 600 K as shown in Figs. 7.4(a-d).

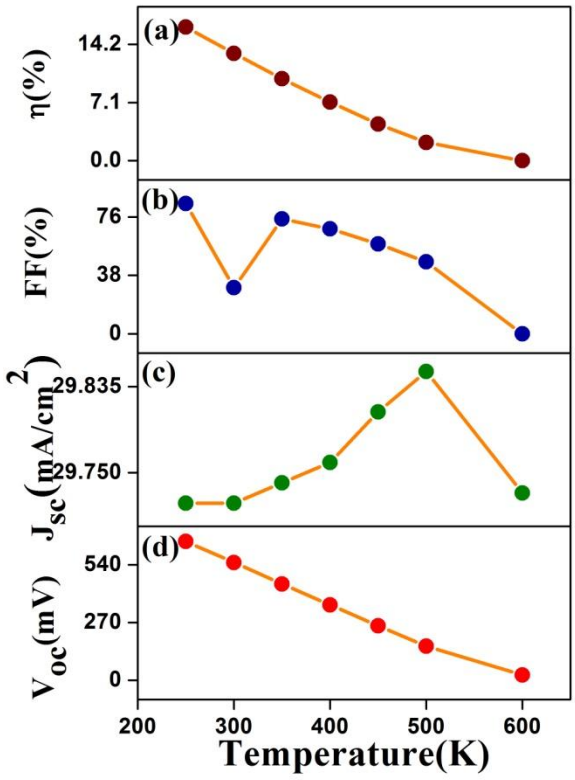

Figure 7.4 Variation in Solar cell output parameters (a) efficiency (b) fill factor(c) Jsc (d) V_{OC} with temperature changes.

V_{OC} is linearly decreased with increase in temperature, which is in accordance with the fact that Voc is directly related to reverse saturation current [56]. Increase in temperature reduces the band gap of silicon and thus increases the reverse saturation current whereas V_{OC} decreases. J_{SC} is found to be constant while the overall η decreases with temperature.

Chapter 8 : Conclusion

We have simulated the proposed TCO(ITO)/ n-WSe_2/p-cSi/Ag heterojunction solar cell using AFORS-HET v2.5 and studied the effect of various material parameters on solar cell output independently. Among all the parameters, N_A/N_D, N_C/N_V, thickness of layers and the layer number of WSe_2 were the ones which influenced the cell efficiency. The output parameters for best optimized solar cell are tabulated as below in Table 3.

After analyzing n-WSe_2 layer parameters, the maximum η of 9.055 % has been achieved. While after optimizing p-c silicon layer parameters, we found that the η was greatly enhanced by increasing reached to 13.09 % maximum at 600 μm. Efficiency 7.55 % was achieved in case commercial silicon of 100 μm thickness. Present results demonstrated that multilayer WSe_2 has acted as an efficient transparent conducting electrode.

Future scope-

The proposed solar cell shows appreciable efficiency and high values of V_{OC} and J_{SC}. Hence, this theoretical model could be further extended to experimental prototype. Also, in this project we did only DC characterization of this device, moreover AC characterization could be done to study PEL, C-V and other characteristics which provide more clarity about the simulated device.

Practical solar cell also has a number of defects and trap levels and non zero series and shunt resistances which can be also modeled using AFORS-HET software. Also surface texturing could be added so as to understand the reflection losses in the solar cell. Further the cell can be optimized for more number of semiconductor layers and the performance can be compared using different substrates with tungsten diselenide.

Table 3. Summary of the best optimized solar cell parameters.

Cell parameters	**n-WSe_2 layer optimized cell**	**n-WSe_2 and p-cSi wafer optimized solar cell**		**p-cSi wafer optimized cell for commercially available silicon cell**
		(@100 μm p -cSi)	(@ 600 μm p-cSi)	
V_{oc} (mV)	472.4	546.1	550.8	474.2
J_{sc} (mA/cm^2)	24.23	26.07	29.72	20.27
FF (%)	79.07	79.64	79.96	78.58
Efficiency (%)	9.055 (@100 μm p-cSi) (@ triple layer WSe_2 at N_D=5×$10^{16}$$cm^{-3}$ at N_C/N_V= 5× 10^{17} cm^{-3}, E_g = 0.9 eV, χ = 3.95 eV, ε_r = 7.2, μ_n = 250 cm^2/Vs and p-cSi at N_A=1×$10^{16}$$cm^{-3}$, N_C/N_V=3×10^{19} cm^{-3} and χ =4 eV)	11.34 (@ triple layer WSe_2 at N_D=5×10^{16} cm^{-3} at N_C/N_V= 5× 10^{17} cm^{-3}, E_g =0.9 eV, χ = 3.95 eV, ε_r = 7.2, μ_n = 250 cm^2/Vs and @ p-cSi at 1×$10^{17}$$cm^{-3}$, N_C/N_V at 1×10^{18} cm^{-3} and χ at 4 eV)	13.09 (@ triple layer WSe_2 at N_D=5×$10^{16}$$cm^{-3}$ at N_C/N_V= 5× 10^{17} cm^{-3}, E_g =0.9 eV, χ = 3.95 eV, ε_r = 7.2, μ_n = 250 cm^2/Vs and @ p-cSi at 1×$10^{17}$$cm^{-3}$, N_C/N_V at 1×10^{18} cm^{-3} and χ at 4 eV)	7.555 @100 μm p-cSi) (@triple layer WSe_2 at N_D=5×$10^{16}$$cm^{-3}$, N_C/N_V=5×$10^{17}$$cm^3$ and E_g = 0.9 eV, χ = 3.95 eV, ε_r = 7.2, μ_n = 250 cm^2/Vs @ p-cSi N_A at 1×10^{17} cm^{-3}, N_C/N_V at 1×10^{18} cm^{-3} and χ at 4 eV

Chapter 9. References

1. ASTM G173 - 03 Reference Spectr http://rredc.nrel.gov/solar/spectra/am1.5/
2. Solar panels :http://toolbox.vetonline.swin.edu.au/13_02/content_sections/learn_about/08_solar_page, 006.htm
3. DSSC: Dye Sensitized Solar Cells, Figure 3, http://www.gamry.com/application-notes/physechem/dssc-dye-sensitized-solar-cells/
4. http://electronicdesign.com/power-sources/what-s-difference-between-thin-film-and-crystalline-silicon-solar-panels
5. http://www.doitpoms.ac.uk/tlplib/semiconductors/junction_rectifying.php
6. http://ecetutorials.com/question-answers/basic-electronics/be6/
7. http://www.thequartzcorp.com/en/blog/2014/09/15/cell-lifetime-and-recombination-part-i/91
8. S. DeWolf, A. Descoeudres, Z. C. Holman, and C. Ballif, "High-efficiency Silicon Heterojunction Solar Cells: A Review", Green **2**, 7–24(2012).
9. I. Khrapach, F.Withers, T. H. Bointon *et al.,* "Novel highly conductive and transparent graphene-based conductors", Adv.Mater. **24**, 2844–2849(2012).
10. S. Bae, H. K. Kim *et. al*., "30 inch Roll-Based Production of High-Quality Graphene Films for Flexible Transparent Electrodes", Nature Nanotechnolog, **5**, 574–578 (2010).
11. R. R. Nair, P. Blake *et al., "*Fine Structure Constant Defines Visual Transparency of Graphene", Science **320**, 1156965(2008).
12. F. Xia,T. Mueller *et al., "*Photocurrent Imaging and Efficient Photon Detection in a Graphene Transistor", *Nano Lett. 9, 1039-1044(2009).*
13. Cheng Gong , Hengji Zhang *et al., "*Band alignment of two-dimensional transition metal dichalcogenides: application in tunnel field effect transistors", Appl. Phys. Lett. **103**, 053513(2013).
14. K. Ghosh , U. Singisetti*, et al.,* "Thermoelectric transport coefficients in mono-layer MoS_2 and WSe_2: Role of substrate, interface phonons, plasmon, and dynamic screening", Appl. Phys. **118**, 135711(2015).

15. W. Liu, J. Kang, *et al.,* "Role of Metal Contacts in Designing High-Performance Monolayer n-Type WSe_2 Field Effect Transistors", *Nano Lett.* **13**, 1983–1990(2013).
16. W. Liu, W. Cao *et al*., "High-Performance Field-Effect-Transistors on Monolayer WSe_2", ECS Transactions **58**, 281-285(2013).
17. D. Jariwala, V. K. Sangwan *et al*., "Band-like transport in high mobility unencapsulated single-layer MoS_2 transistors", App. Phy. Lett. **102**, 173107(2013).
18. J. Huang, L. Yang *et al*., "Large-area Synthesis of Monolayer WSe_2 on SiO_2/Si Substrate and its Device Applications", **Nanoscale 7**, 4193-4198(2015).
19. H. J. Chuang, X. Tan, *et al*., "High Mobility WSe_2 p- and n-Type Field-Effect Transistors Contacted by Highly Doped Graphene for Low-Resistance Contacts", *Nano Lett.,***14**, 3594–3601(2014).
20. I. Lee, S. Rathi, *et al*., "Non-degenerate n-type doping by hydrazine treatment in metal work function engineered WSe_2 field-effect transistor", Nanotechnology **27**, 225201(2016).
21. Komsa, Hannu-Pekka, and Arkady V. Krasheninnikov. "Electronic structures and optical properties of realistic transition metal dichalcogenide heterostructures from first principles." Physical Review B **88.8** , 085318(2013).
22. Wang, Qing Hua, et al. "Electronics and optoelectronics of two-dimensional transition metal dichalcogenides." Nature nanotechnology **7.11** ,699-712(2012)
23. Gmelin, "Gmelin handbook of inorganic and organometallic chemistry" ,Springer Verlag, Berlin (1995).
24. Zibouche, Nourdine, et al. "Transition-metal dichalcogenides for spintronic applications." Annalen der Physik 526.9-10 (2014): 395-401.
25. Investigation of optical properties of WSe_2, $W0.9Se_2$ and $MoSe_2$ single crystals,Shodhganga p-139(2009).
26. Liu, Wei, et al. "Synthesis of high-quality monolayer and bilayer graphene on copper using chemical vapor deposition." Carbon **49.13** ,4122-4130(2011).
27. J. Huang, L. Yang *et al*., "Large-area Synthesis of Monolayer WSe_2 on SiO_2/Si Substrate and its Device Applications", **Nanoscale 7**, 4193-4198(2015).
28. G. Clark, S. Wu *et al*., "Vapor-transport growth of high optical quality WSe_2 monolayers", App. Phy. Lett. **2**, 101101(2014).

29. Jariwala, Deep, et al. "Emerging device applications for semiconducting two-dimensional transition metal dichalcogenides." ACS nano **8.2** ,1102-1120(2014). R.Stangl, M.Kriegel et al., "AFORS-HET, Version 2.2, a Numerical Computer Program for Simulation of Heterojunction Solar Cells and Measurements", IEEE **2**, 1350 – 1353(2006).
30. Froitzheim, A., et al. "AFORS-HET: a computer-program for the simulation of heterojunction solar cells to be distributed for public use." Photovoltaic Energy Conversion, 2003. Proceedings of 3rd World Conference on. Vol. 1. IEEE, 2003.
31. Mryasov, O.N.; Freeman, A.J. Electronic band structure of indium tin oxide and criteria for transparent conducting behavior. Phys. Rev. B 2001, 64, 233111–233113.
32. Sugiyama, K.; Ishii, H.; Ouchi, Y.; Seki, K. Dependence of indium–tin–oxide work function on surface cleaning method as studied by ultraviolet and x-ray photoemission spectroscopies. J. Appl. Phys. 2000, 87, 295: 1–295: 4.
33. Park, Y.; Choong, V.; Gao, Y.; Hsieh, B. R.; Tang, C.W. Work function of indium tin oxide transparent conductor measured by photoelectron spectroscopy. Appl. Phys. Lett. 1996, 68, 2699–2701.
34. Park, Yongsup, et al. "Work function of indium tin oxide transparent conductor measured by photoelectron spectroscopy." Applied Physics Letters 68.19 (1996): 2699-2701.
35. Alam, M. J., and D. C. Cameron. "Optical and electrical properties of transparent conductive ITO thin films deposited by sol–gel process." Thin solid films 377 (2000): 455-459.
36. Benamar, E., et al. "Structural, optical and electrical properties of indium tin oxide thin films prepared by spray pyrolysis." Solar Energy Materials and Solar Cells 56.2 ,125-139(1999).
37. Michaelson, Herbert B. "The work function of the elements and its periodicity." Journal of Applied Physics 48.11 (1977): 4729-4733.
38. Kam, Kam-Keung, "Electrical properties of WSe_2, WS_2, $MoSe_2$, MoS_2, and their use as photoanodes in a semiconductor liquid junction solar cell" ,Retrospective Thesis and Dissertations. Paper 8356(1982).
39. K. Kim, S. Larentis, et al., "Band Alignment in WSe_2-Graphene Heterostructures", *ACS Nano* **9**, 4527–4532(2015).

40. H. Fang , S. Chuang et al., "High Performance Single Layered WSe_2 p-FETs with Chemically Doped Contacts", *Nano Lett.* **12**, 3788–3792(2012).
41. S. Zhong, X. Hua,W. Shen et al., "Simulation of high-efficiency crystalline silicon solar cells with homo–hetero junctions ", IEEE Trans. on Electron Devices **60**, 2104-2110(2013).
42. U. Gangopadhyay, S. Roy, S. Garain et al., "Comparative simulation study between n-type and p- type silicon solar cells and the variation of efficiency of n- type solar cell by the application of passivation improvement layer with different thickness using AFORS HET and PC1D", IOSR Journal of Engineering **2(8)**, 41-48(2012).
43. Z. Zhang, T. Cui, et al., "Improved efficiency of graphene/Si heterojunction solar cells by optimizing hydrocarbon feed rate", Journal of Nanomaterials **2014**, 359305 (2014).
44. D. Cheyns, J. Poortmans *et al*., "Analytical model for the open-circuit voltage and its associated resistance in organic planar heterojunction solar cells", Physical Review **B 77**, 165332(2008).
45. Wilfried G.J.H.M., V. Sark, *et al*., "Physics and Technology of Amorphous-Crystalline Heterostructure Silicon Solar Cells", 197-395(1997).
46. M. Dadu, A. Kapoor, *et al*., "Effect of operating current dependent series resistance on the fill factor of a solar cell", Solar Energy Materials a Solar Cells **71**, 213–218 (2002).
47. S. Sokolic, S. Amon.,"Modelling heavy doping effects for low temperature device simulations", Journal de Physique IV Colloque, **04** (C6),133-138(1994).
48. R. R. King, R. A. Sherif, *et al*., "Bandgap Engineering in High-Efficiency Multijunction Concentrator Cells", 3rd International Conference on Solar Concentrators (ICSC-3), Scottsdale, AZ, May(2005).
49. I. Lee, S. Rathi, *et al*., "Non-degenerate n-type doping by hydrazine treatment in metal work function engineered WSe_2 field-effect transistor", Nanotechnology **27**, 225201(2016).
50. J. T. Shieh, C. Hua Liu *et al*., "The effect of carrier mobility in organic solar cells", Journal of Appl. Phy. **107**, 084503(2010).
51. J. M.Gee, M.D. Bode,*et al*., "Boron-Doped Back-Surface Fields Using an Aluminum-Alloy Process", 26th IEEE PVSC, 275-278(1997).

52. W. Liu, W. Cao *et al*., "High-Performance Field-Effect-Transistors on Monolayer WSe_2", ECS Transactions **58**, 281-285(2013).
53. Haque, KASM Ehetshamul, *et al.*, "An analysis of efficiency variation in an Al0. 7Ga0. 3As/Al0. 48In0. 52As heterojunction solar cell with change in device parameters using adept 1D software.",Electronic Materials Letters **9.1**, 47-52(2013).
54. Tsai, M.L., *et al.*, "Monolayer MoS_2 heterojunction solar cells.", ACS nano **8(8)**, 8317-8322(2014).
55. S. Chander , A. Purohit *et al*., " A Study on Spectral Response and External Quantum Efficiency of Mono-Crystalline Silicon Solar Cell", International Journal of Renewable Energy Research **5**,1(2015).
56. A. El-Shaer, M. T. Y. Tadros *et al*.," Effect of Light intensity and Temperature on Crystalline Silicon Solar Modules Parameters", International Journal of Emerging Technology and Advanced Engineering **4**, 2250-2459(2014).
57. P. Kumar, S. C. Jain *et al*., "Effect of illumination intensity and temperature on open circuit voltage in organic solar cells", Appl. Phy. Lett. **94**, 183505(2009).